HHS Public Access

Author manuscript

Phys Med Biol. Author manuscript; available in PMC 2018 October 04.

Published in final edited form as:

Phys Med Biol. ; 62(20): R207–R235. doi:10.1088/1361-6560/aa8b31.

Modelling the transport of optical photons in scintillation detectors for diagnostic and radiotherapy imaging

Emilie Roncali[1], **Mohammad Amin Mosleh-Shirazi**[2,*], and **Aldo Badano**[3]

[1]Department of Biomedical Engineering, University of California Davis, Davis, USA

[2]Medical Imaging Research Center, and, Physics Unit, Department of Radiotherapy and Oncology, Namazi Hospital, Shiraz University of Medical Sciences, Shiraz 71936-13311, Iran

[3]Office of Science and Engineering Laboratories, Center for Devices and Radiological Health, U.S. Food and Drug Administration, Silver Spring, MD 20852, USA

Abstract

Computational modelling of radiation transport can enhance the understanding of the relative importance of individual processes involved in imaging systems. Modelling is a powerful tool for improving detector designs in ways that are impractical or impossible to achieve through experimental measurements. Modelling of light transport in scintillation detectors used in radiology and radiotherapy imaging that rely on the detection of visible light plays an increasingly important role in detector design. Historically, researchers have invested heavily in modelling the transport of ionizing radiation while light transport is often ignored or coarsely modelled. Due to the complexity of existing light transport simulation tools and the breadth of custom codes developed by users, light transport studies are seldom fully exploited and have not reached their full potential. This topical review aims at providing an overview of the methods employed in freely available and other described optical Monte Carlo packages and analytical models and discussing their respective advantages and limitations. In particular, applications of optical transport modelling in nuclear medicine, diagnostic and radiotherapy imaging are described. A discussion on the evolution of these modelling tools into future developments and applications is presented.

Keywords

Scintillation detectors; Monte Carlo simulation; light transport; optical Monte Carlo; diagnostic imaging; image-guided radiotherapy; optical modelling

[*]**Author for correspondence:** MA Mosleh-Shirazi PhD, Physics Unit, Radiotherapy & Oncology Department, Namazi Hospital, Shiraz University of Medical Sciences, Shiraz 71936-13311, Iran, Tel: +98 71 3612 5316, Fax: +98 71 36474320, mosleh_amin@hotmail.com & amosleh@sums.ac.ir.

The authors declare equal leadership and contribution regarding this review.

Conflict of interest: None

1 Introduction

The term *radiation transport* refers to the generation and tracking of interactions by a particle or ray and produced secondary particles. Modelling of the radiation transport enhances the understanding of the relative importance of individual processes involved in imaging and leads to design improvements that would be impractical or impossible to achieve through merely experimental measurements. In this topical review, we describe the role of optical transport modelling in the context of scintillation detectors used in medical imagers for detection of gamma- and X-rays. We provide an overview of the general principles common to such detectors including the physics of scintillation, approaches to modelling and validation, and computational speed and efficiency, and describe relevant research in the three disciplines of diagnostic X-ray imaging, nuclear medicine and radiotherapy imaging). We introduce types of medical detectors where visible light is involved in the detection process, highlight the importance of light transport in the overall efficiency and quality of the imaging, present the rationale and motivation for modelling optical photon transport for detector optimization, and provide a historical overview of the research in this field. Although the main emphasis is placed on imaging detectors, research performed in other relevant areas is also briefly mentioned for context and completeness.

1.1 Medical imaging detectors involving light detection

Scintillators are used in many medical imaging instruments. With high density and high light yield, scintillators are good candidates for applications where high detection efficiency for × and gamma rays and high pixel signal-to-noise ratio (SNR) are required. Scintillator-based imagers require a light-detection sensor (photodetector) that forms an image using collected light. The SNR of the photodetection process primarily depends on the magnitude and spatial distribution of the energy deposited by the incident ionizing particles and on numerous other factors including the scintillation yield, the optical properties of the scintillator material and applied coatings, the probability of photons to reach the photodetector, the photodetector spectral quantum efficiency, and the statistics of the charge carrier distribution (Knoll, New scintillators and photodetectors are produced for various applications (Van Eijk, 2008). How a scintillator is used in a detector depends on the intended application of the imager. Design parameters include the imaging configuration, the choice of scintillator and its geometry, and the method of scintillation light detection (including the choice of photodetector and optical coupling). Table 1 summarizes the main design parameters for instruments that have been studied in five medical imaging applications. The first two are used in nuclear medicine: gamma cameras for planar imaging and single photon emission computed tomography (SPECT), and positron emission tomography (PET) scanners. The next two are used in diagnostic imaging: digital radiography (DR) and kilovoltage X-ray computed tomography (kVCT) systems. The final column refers to megavoltage X-ray computed tomography (MVCT) scanners designed for radiotherapy treatment verification. A variety of solid scintillators in monolithic (single block), pixelated (segmented), unstructured, columnar, or thin-screen geometries have been studied. The photodetectors constitute arrays of photomultiplier tubes (PMTs) or silicon photomultipliers (SiPMs) in gamma-ray detectors and arrays of amorphous silicon (a-Si)

photodiodes, charge-coupled devices (CCDs), or complementary metal–oxide–semiconductors (CMOS) devices in X-ray imagers.

1.2 Motivation for modelling light transport in scintillators

The use of modelling, and in particular Monte Carlo (MC) simulations, is well established in medical imaging research. This stems from the flexibility such models offer and the ability they provide to compute otherwise unobtainable quantities of interest. Historically, researchers have invested a lot of effort on modelling the transport of primary ionizing radiation and secondary ionizing particles or rays they produce upon passage through various media of interest in radiation physics and dosimetry. In addition to many analytical solutions, various detailed ionizing-radiation MC simulation packages have resulted from these efforts, for example, EGSnrc, PENELOPE, MCNP, FLUKA, GEANT4, SIMSET, and VMC^{++} (Rogers, 2006).

The detection process in scintillators, however, includes events that involve both ionizing radiation (gamma rays, X-rays, electrons, positrons) and optical photons. In the majority of reported modelling studies on medical scintillator-based detectors, an ionizing radiation-only approach is taken (Swindell and Evans, 1996; Sawant *et al.*, 2005; Liu *et al.*, 2012; Wang *et al.*, 2008; Wang *et al.*, 2010). Conclusions are then made without accounting for light transport or, in some cases, using non-validated or not fully disclosed optical models. Including proper light transport in simulations, such as light absorption and scattering in the detector, crystal microstructure, scintillator coating type and reflectivity, and angular distribution of the light exiting the crystal, will affect some parameters that may influence detector or system optimization (Mosleh-Shirazi *et al.*, 1998a; Badano and Sempau, 2006; Monajemi *et al.*, 2006; Wang *et al.*, 2009; Roncali and Cherry, 2013; Mosleh-Shirazi et al., 2014a, 2014b; Nillius *et al.*, 2015). The significantly limited availability and specialized nature of optical MC code compared to ionizing radiation MC packages has contributed to their less frequent use.

Another important feature of optical MC codes is that they often allow researchers to control parameters to provide insight into system behavior. For instance, an input parameter such as a monochromatic wavelength can be kept constant while the magnitude of interesting quantities (e.g., number and angles of reflection from a particular surface) can be sampled in a controlled way. Moreover, contributions from different processes can be separated (e.g., light absorption in crystal coating versus bulk absorption, scintillation emission time and light transit time in the crystal, etc.) (Mosleh-Shirazi *et al.*, 1998a; Roncali *et al.*, 2014). However, in some general-purpose optical MC codes, detailed information on quantities of interest describing the history of the light rays are not always accessible, making in-house codes with complete access and flexibility still attractive (Mosleh-Shirazi *et al.*, 2014a).

A further advantage is the time and cost savings offered by computer models. Optimization of scintillation crystals requires changing many parameters resulting in a large number of combinations. To do this experimentally is costly and time-consuming (Roncali *et al.*, 2014).

1.3 Brief overview of the history of optical modelling for medical imaging detectors

Motivated by the additional insight that optical modelling provides, various groups have developed MC codes or analytical models that can simulate light transport in scintillators. Initial work was carried out for non-medical radiation physics applications. One of the earliest reported computer-based models studied cylindrically symmetric scintillators such as those used in lens spectrometers for electrons (Falk and Sparrman, 1970). During the following two decades, optical simulation was used to design scintillation counters and imaging systems in nuclear medicine and study the energy resolution of scintillation counters (Schölermann and Klein, 1980), optical coupling between scintillator and PMT (Derenzo and Riles, 1982), and improvement of light collection efficiency from scintillators (Carrier and Lecomte, 1990; Knoll and Knoll, 1988). A number of further reports on optical MC simulations in nuclear imaging appeared in the following decade including work on light collection in scintillators with rough or diffuse surfaces (Baranov *et al.*, 1996; Bea et al., 1994a), small or narrow crystal geometries (Cherry *et al.*, 1995; Ordonez *et al.*, 1997), and energy resolution of multicrystal encoding detectors (Vozza *et al.*, 1997). More recent examples of optical MC research on nuclear imaging using gamma cameras include compact gamma cameras based on avalanche photodiodes (Després *et al.*, 2007), dedicated brain SPECT model (Hirano *et al.*, 2012) and faster MC computation (Hunter *et al.*, 2013). A larger number of papers were published on PET including work on monolithic scintillation crystals (van der Laan *et al.*, 2010b; Vinke and Levin, 2014), crystal surface characterization (Roncali and Cherry, 2013b; Yang *et al.*, 2013), and temporal resolution for time-of-flight (TOF) PET (Berg *et al.*, 2015; Derenzo *et al.*, 2014, 2015; Moses *et al.*, 2014; Roncali *et al.*, 2014).

As for X-ray detector optimization, the first papers on optical transport MC modelling were published in the 1990s for optimization of a thin phosphor screen employed in an electronic portal imaging device (EPID) (Radcliffe *et al.*, 1993) and as a tool for developing a thick, high quantum efficiency (QE) scintillation detector (Mosleh-Shirazi *et al.*, 1994) for an early prototype EPID and cone-beam MVCT scanner for radiotherapy verification (Mosleh-Shirazi *et al.*, 1998b; Mosleh-Shirazi et al., 1998c) (Figure 1). Experimental validation of the latter model, its applications, updated versions and further benchmarking have also been reported (Mosleh-Shirazi *et al.*, 1998a, 2014a, 2014b; Ranjbar, 2015). Optimization of other types of segmented crystalline detectors using optical MC modelling has also been a topic of interest (Monajemi *et al.*, 2006; Wang *et al.*, 2009), as has optical MC simulation for dosimetric use of EPID images (Blake *et al.*, 2013).

The field of diagnostic X-ray imaging has also seen a significant development and use of optical MC modelling. Indirect imaging systems employing columnar scintillators (e.g., cesium iodide) have been studied in a series of experimentally verified dedicated optical MC codes (Badano and Sempau, 2006; Freed *et al.*, 2009; Sharma *et al.*, 2012; Sharma and Badano, 2013; Dong *et al.*, 2014; Nillius *et al.*, 2015).

Analytical models and numerical simulations have also been applied to optical modelling (Swindell, 1991; Swindell *et al.*, 1991; Evans *et al.*, 2006; Freed *et al.*, 2010; Poludniowski et al., 2013a; Poludniowski et al., 2013b).

1.4 Challenges in modelling optical transport in scintillation detectors

The total number of ionizing radiation and optical events that have to be simulated to reduce the uncertainty in the results to acceptable levels can be extremely high. According to Sharma et al., a clinical exposure level would necessitate modeling of the order of 10^{21} events including detailed tracking of primaries and all secondaries (Sharma *et al.* 2012). In most cases, it is not necessary to model in detail all of the scattering processes. However, in order to achieve estimates within a reasonable uncertainty band (1-5%), simulations often require running 10^{10} - 10^{12} primary histories and all of the associated optical photons resulting from the deposition of energy in the scintillator layers. Although computation speed is continuously increasing, introducing all of the realistic but complicating processes to be simulated in a particle history still remains challenging given the need to obtain results faster. This is one of the reasons why existing codes typically include optical transport in a simplified way. Simplifications may include rudimentary detector geometry and surface treatment descriptions (e.g., surface roughness, angular distribution of reflected light, probability of crosstalk, etc.), unrealistic distribution of depths of optical photon generation, assuming single-wavelength scintillation light and using mean optical quantities ignoring spectral distributions and polarization states.

Accurate modelling of optical photon transport inside and outside a scintillator remains challenging particularly when insufficient detail is available or provided with respect to randomness in the microcolumnar structure of scintillators and surface roughness. There is still a need for better characterized phosphor screen optics, optical crosstalk in multi-element scintillator arrays, and more generally optical transport in coupling media and photodetectors. Further experimental validation and benchmarking is also challenging and required.

1.5 Goals of this review

This topical review provides an overview of the methods employed in freely available, open-source and in-house, optical MC packages and discuss their respective advantages and limitations. In particular, applications of optical transport modelling in nuclear medicine and diagnostic and radiotherapy X-ray imaging are described. A discussion on future directions of interest is also presented.

2 Light transport in scintillation detectors

2.1 Basic principles

Scintillation detectors are traditionally composed of a scintillator coupled to a photodetector. The detection of a high energy photon (γ or X-ray) can be divided in three stages described in Figure 2. First, the role of the scintillator is to stop the incident high energy photon and produce visible light by scintillation generally within 10-1000 ns (Derenzo *et al.*, 2003). Light intensity is approximately proportional to the energy deposited by the incident ionizing radiation. Second, the scintillation light is transported in a structured that might be covered with a reflective material. Third, light is collected by the photodetector and converted into an electrical signal. The amplitude of the signal is proportional to the amount of light and, therefore, to the energy deposited by the interaction of the incident photon with

the scintillator. Optimizing the scintillation process, optical transport, and light collection are all essential aspects of detector design.

The scintillation depends on the intrinsic properties of the scintillator and external factors including temperature (Dorenbos *et al.*, 1995). Characteristics of common scintillator materials are given in section 2.2. Light transport is determined both by intrinsic optical properties and surface reflectance properties. The scintillation light bounces on crystal surfaces until it either reaches the photodetector or escapes. Alternatively, it may also get internally scattered or absorbed. The basic physics principles are described in section 2.3. Collecting a maximum amount of scintillation light is critical for energy, timing and contrast resolutions. Once light reaches the photodetector sensitive layer, it is converted into photoelectrons with an efficiency characteristic of the photodetector employed and the geometrical arrangement of the scintillator and photodetector. Various coupling strategies have been developed, using light guides, direct coupling, or remote light collection. Photodetectors and optical coupling are described in section 2.4.

2.2 Light production and scintillator properties

2.2.1. Scintillators—High energy radiation is converted into visible light by a scintillator or phosphor (Cherry *et al.*, 2012b). In scintillators, the primary conversion mechanism is fluorescence (luminescence from singlet-singlet relaxation) and there is only a small phosphorescence component (luminescence from triplet-singlet relaxation). Phosphorescence is typically characterized by a longer decay time and results in a slow component often not desired in scintillators. In contrast, phosphors include all materials that exhibit radioluminescence. While thin phosphors (100-400 microns) can be used for detection of X-rays (10-100 keV), thicker scintillators (>5 mm) with high stopping power are needed for detection of higher energy gamma and X-rays (>100 keV). Many detectors employ inorganic scintillators with a crystalline structure that usually require impurities. These impurities are responsible for the scintillation emission and are called emission centers (Derenzo *et al.*, 2003). Inorganic scintillators are typically grown in boules using pull-down methods or the Czochralski process. The nature of the crystal and impurity or doping material determine important optical properties such as light yield, index of refraction, emission spectrum, and kinetics (Derenzo *et al.*, 2014). For example, sodium iodide activated with thallium (NaI(Tl)) is the most commonly used scintillator in gamma cameras and SPECT systems to detect gamma rays ranging from 50 to 250 keV. Denser materials such as bismuth germanium oxide (BGO), or lutetium oxyorthosilicate doped with cerium (LSO:Ce) are used for detection of 511 keV gamma photons produced by positron annihilation in PET. LSO:Ce, a scintillator discovered in the 1990s (Melcher and Schweitzer, 1992) is now used in the majority of commercial PET scanners. High density scintillators (e.g., CsI(Tl), $CdWO_4$, $ZnWO_4$ and BGO) are normally required for detection of megavoltage photons. A high light yield (number of light photons generated per unit energy absorbed) is another property of interest in most applications. CsI(Tl) has the highest light yield among common inorganic scintillators (65 photons/keV).

Most scintillators have a high index of refraction (e.g., 1.85 for NaI, 1.82 for LSO, 2.15 for BGO and 2.3 for $CdWO_4$) (Knoll, 2000) resulting in low-efficiency optical coupling to the

photodetector which entrance window is usually made of glass or epoxy with a lower index of refraction (1.5). The majority of scintillators emit visible light with a broad spectrum that extends in the UV (Cherry *et al.*, 2012a). CsI(Tl), BGO, LSO:Ce and NaI(Tl) emission peaks are located at 540 nm, 480 nm, 420 nm and 415 nm, respectively (see Figure 3). The emission spectrum affects optical detection efficiency due to the amount of overlap with the absorption spectrum of a given photodetector. Recently, a new class of scintillators called garnet ceramics has gained interest with high density, good optical properties and relatively low production cost (Wang *et al.*, 2012). These ceramics have an emission peak in the yellow part of the spectrum (545 nm) which requires adapted photodetectors.

The rise and decay time of a scintillator are particularly important where coincidence detection relies on the detectors' ability to detect gamma photons within a few tens of nanoseconds (as in PET). To achieve high timing resolution, scintillators with fast rise time and decay times are desirable. BGO has been used in PET scanners for several decades but has a rather long decay time of 300 ns, making it less ideal for time-of-flight capability (TOF) applications (Moses and Derenzo, 1999; Knoll, 2000). Because of their attractive timing properties and light yield, LSO and variants such as LYSO (lutetium yttrium oxyorthosilicate) have replaced BGO in most recent scanners. Timing is less critical in gamma cameras, SPECT and X-ray imaging as they are not operated in coincidence mode (Knoll, 2000). Materials with no or low amounts of "afterglow" from long-lived decay components are, however, preferred in high-rate dynamic and fast tomographic imaging.

2.2.2. Phosphors—In a typical digital radiography detector, a thin layer of phosphor is deposited on a large-area photodiode. Phosphor screens are traditionally made of a phosphor powder mixed with glue and coated onto a substrate with a reflective layer on the front face (Figure 2, right). These phosphors are high-density materials such as gadolinium oxysulfide doped with terbium or Europium (Gd_2O_2S:Tb or GOS:Tb, GOS:Eu) or zinc sulfide (ZnS:Ag) designed to stop 10-keV to 100-keV X-rays (Liaparinos *et al.*, 2006). The stopping power depends on particle size (2.5-50 μm), packing fraction, as well as on the density and atomic number of the phosphor. Emission spectra typically peak in the yellow. These phosphors also have high refractive indices (2.4 for GOS and ZnS:Ag). GOS produces an average of 50 light photons/keV (Carel, 2002).

2.3 Photon transport in a scintillation crystal

Because of fundamental differences in material structure and geometry, light transport in scintillators and phosphors can be very different. This section describes the basic principles of optical transport in a thick scintillation crystal (Figure 2, left). The interaction of the incident high energy photon produces thousands of visible photons (e.g., 5-50 per keV (Cherry *et al.*, 2012a)) with emission times distributed along a decreasing exponential characteristic of the scintillator (Melcher and Schweitzer, 1992). Scintillation photons can be reflected, refracted or absorbed at crystal surfaces and absorbed or scattered in the crystal (Mosleh-Shirazi *et al.*, 1994, Moisan *et al.*, 1997). Self-absorption and bulk scattering should be limited to ensure high light output. Bulk scattering is mainly due to changes in refractive index created by impurities. Other types such as Rayleigh scattering by particles much smaller than the wavelength of the scintillation light are typically negligible.

2.3.1. Reflections in the crystal—Scintillation detectors use either arrays of small and long crystals or large monolithic crystals. In thick and narrow crystals (e.g., 1-5 mm cross sectional area and 10-30 mm thickness), most photons undergo multiple reflections on the crystal sides. In this case, surface reflection properties play a larger role in light transport. When a photon reaches the crystal surface at a certain angle of incidence, the photon can be transmitted or reflected with respect to the local orientation of the crystal surface (Figure 4). The probabilities of reflection (R) and transmission corresponding to the incidence angle θi (Eq. 1) can be calculated using Fresnel equations for unpolarized light (Levin and Moisan, 1996). The reflection probability is described using Fresnel equations. By expressing θ_t as a function of θ_i using Snell's law with the crystal index of refraction n_i and the outer medium index of refraction n_t ($n_i \sin \theta_i = n_t \sin \theta_t$), R can be expressed solely as a function of n_i, n_t, and θ_i. Photons with an angle of incidence higher than the critical angle given by Snell's law will be subject to total internal reflection. Reflection properties of such crystals can be characterized considering the reflectivity of the surface constant. More sophisticated models for non-flat surfaces describe the reflectivity as a function of photon incidence angle (Janecek and Moses, 2010; Roncali *et al.*, 2013).

$$R=\frac{1}{2}\left[\frac{\sin^2(\theta_i-\theta_t)}{\sin^2(\theta_i+\theta_t)}+\frac{\tan^2(\theta_i-\theta_t)}{\tan^2(\theta_i+\theta_t)}\right] \quad (1)$$

The reflectance properties can be tuned through surface treatment (Huber *et al.*, 1999). Common surface finishes include mechanical polish, chemical etch, or "ground". All these surface treatments are applied to saw-cut crystals that present a rough and uneven surface with height variation of several microns. Mechanically polished crystal faces have a high degree of flatness with variations of 100 nm or less. In spite of imperfections such as roughness and scratches, these surfaces behave similarly than ideal flat surfaces reflecting a large fraction of the impinging light. Chemical etching adds a degree of polishing to rough surfaces that can be controlled by etching time and chemicals used (Huber *et al.*, 1999; Slates *et al.*, 2000). Etching has been shown to improve light output (defined as the ratio of detected to emitted scintillation photons) most likely because it reduces the number of reflections that each photon undergoes. The total probability, p, of a given scintillation photon reaching the photodetector after N reflections is a direct function of the reflection coefficient, R, elevated to the power of the number of reflections N:

$$p=(1-R)^N \quad (2)$$

For example, even with a high probability of reflection of 98%, a photon undergoing 20 reflections only has 67% chance of reaching the photodetector.

On the other end of the spectrum, saw-cut and ground surfaces with high degree of roughness are better described by an ensemble of microfacets with varied orientation around the nominal surface. Reflectance properties of such crystals are much more complex to describe analytically. Some effort has been placed in measuring or computing the reflectance

based on experimental surface data (Janecek and Moses, 2009; Roncali and Cherry, 2013a) as illustrated in Figure 5 and further described in section 3.2.

Monolithic crystals have larger cross sectional areas than crystals used in arrays (typically 20 mm vs. 4 mm) decreasing the number of reflections on the crystal sides. However, surface treatment remains a critical factor in obtaining accurate positioning of the events within the crystal when not using a collimator. Here, event positioning no longer relies on identification of individual crystals in a detector block but rather on the light spread estimate. Event positioning and spatial resolution are dependent on the thickness of the crystal (Miyaoka *et al.*, 2010). In monolithic crystals, photons travel longer between two reflections on the surfaces and, therefore, have a higher chance of being absorbed or scattered, which reinforces the effect of the scattering and self-absorption coefficients.

2.3.2 Microcolumnar scintillators—In these scintillators commonly used in X-ray detectors and more recently SPECT detectors, light transport is dominated by the reflections in columns of typically 10 μm diameter (Sabet *et al.*, 2012) and subsequent light transmission between columns.

2.3.3. Granular phosphor screens—The light transport is largely dominated by the interaction of the light with the phosphor grains and binder materials. Assuming a homogenous distribution of the microscopic phosphor grains, the light scattering and absorption can be described by the Mie theory (van de Hulst, 1957). Reflections at the boundaries are described by Fresnel equations.

2.3.4. External reflector—As crystals in arrays are tightly packed together, a reflector is placed between the crystals to prevent the light escaping to enter a neighboring crystal. This phenomenon, called optical crosstalk, can decrease spatial resolution, energy resolution and identification of individual crystals in an array. Reflectors are thin specular or diffuse materials (e.g., enhanced Specular Reflector, 3M, or Teflon, Toray) of a few tens of microns. Ideal materials would be purely specular or purely Lambertian (i.e., a diffusely reflecting surface with emitted light intensity proportional to the cosine of the emission angle). However, reflectors often have a Lambertian and a glossy component (Janecek and Moses, 2008b) which makes modelling not able to accurately predict the angular distribution of the reflected light. In addition, the method of attaching the reflector to the crystals also affects reflection properties. Reflectors can be glued, coated (e.g., TiO_2), or coupled with a layer of air (e.g., Teflon tape wrapped around the scintillator). Depending on the index of refraction of this coupling medium, the fraction of light that escapes the scintillator increases resulting in more photons reaching the reflector. Photons travel back and forth between the reflector and the crystal. Some may be ultimately reflected back in the crystal resuming their transport. Other photons might be transmitted through the reflector after multiple reflections between the reflector and the crystal.

Modelling the combination of the crystal optical properties with the reflector adds complexity to simulation models. In monolithic crystals, surface treatment plays a key role in determining spatial resolution by modifying the light spread. Faces are usually covered with a reflector. NaI(Tl) crystals used in gamma cameras or SPECT systems are traditionally

covered with a reflector such as TiO_2 to increase light output. Thin films used in digital radiography flat panel or CT detectors have their front face (opposite to the photodetector) covered with a reflector to redirect light toward the photodetector.

2.4 Light collection and detection efficiency of the photodetector

The coupling of the scintillator to the photodetector is highly dependent on the size of the scintillator and the photodetector, the photodetector pixelation (if any), the change in index of refraction of the scintillator and photodetector entrance face.

2.4.1. Photodetectors—Traditionally, large area crystals for nuclear medicine detectors are read out using an array of photomultiplier tubes (PMTs). Modern gamma cameras use a hexagonal pattern of 30 to 100 PMTs with an average diameter of 5 cm. Traditional PET systems used block detectors based on a pixelated scintillator readout by a 2 × 2 array of PMTs. Recent PET scanners are now based on silicon photomultipliers (SiPMs), a more compact photodetector (Roncali and Cherry, 2011). An important factor in selecting a photodetector is the overlap of the spectral QE with the emission spectrum of the scintillator. Manufacturers have developed PMTs and SiPMs with a QE tailored to the most common scintillators. SiPM have higher photodetection efficiency (PDE) than PMTs (Roncali and Cherry, 2011) in the yellow (typically 30% instead of 10%), but the PDE depends not only on the bulk QE but also on the packing fraction (fill factor), as commercial SiPMs are typically arrays of 3 mm × 3 mm devices.

2.4.2. Scintillator-photodetector coupling—A thin light guide made of acrylic or glass is often used to spread the light exiting the crystal onto the photosensitive area (Kolb *et al.*, 2010). The light guide creates one additional optical interface between the high index crystal (typical 1.8-2.3) and the lower index materials such as glass or acrylic (approximately 1.5), which may decrease light extraction. Gamma camera detectors made with NaI(Tl) crystals that are hygroscopic are encapsulated in a sealed aluminum casing with a glass entrance window. It is not always possible to directly couple the scintillator to the photodetector. In the case of combined PET and magnetic resonance (MR) imaging systems, photodetectors often need to be placed outside of the magnetic field. Such PET detectors have been coupled to the PMTs using optical fibers (Catana *et al.*, 2006).

2.4.3. Remote light detection—Optical minification is required when the imaging system employs a large-area scintillator and there is a limitation on the cross-sectional area and/or the complexity of the optical receptor. The imaging systems in which this method has been most widely used are the so-called video-based EPIDs as one of the initial designs for megavoltage imaging in radiotherapy. Such EPIDs employ a metal-phosphor or metal-scintillator combination as the X-ray convertor and a mirror-lens-camera combination as a remote optical detector. A lens focuses the light to form an image on the CCD. Given the very small size ratio between the CCD and the scintillator and the tradeoffs that exist between the lens *f* number, field of view, and light collection efficiency, a distance of the order 100 cm is required between the scintillator and the lens. This geometry is relatively low cost but suffers from an extremely low optical coupling efficiency (of the order

0.001%). Maximizing the number of optical photons reaching the CCD per X-ray incident on the detector, therefore, becomes important (Swindell 1991, Boyer *et al.*, 1992).

3 A review of light transport simulation tools

3.1 Analytical models

Analytical approximations of light transport have been successfully developed for phosphor and scintillator screens utilized in indirect X-ray imaging systems to convert X-ray photons into light quanta. In X-ray imaging, the absorption of incident X-ray energy takes place at different depths inside the phosphor or scintillating material. This absorbed energy is converted into light photons that travel within a thick slab of phosphorescence material until they hit a sensor layer. The stochastic variations in energy deposition depth, light generation, and light transport processes determine how signal and noise are transferred through the detector. Many investigators have studied the effect of light transport on overall image quality of photographic (Berg, 1969; De Belder *et al.*, 1965; DePalma and Gasper, 1972; Wolfe *et al.*, 1968) and radiographic (Cavouras *et al.*, 2000; Drangova and Rowlands, 1986; Gasper, 1973; Kandarakis and Cavouras, 2001; Lubberts, 1968; Van Metter and Rabbani, 1990; Nishikawa and Yaffe, 1990; Swank, 1973; Antonuk, 2002; Swindell *et al.*, 1991; Wowk *et al.*, 1994) imaging systems. Early work on scintillator screens relied on assumptions that allowed analytical solutions. Swank (Swank, 1973) presented exact and approximated solutions for the line-spread and modulation transfer function (MTF) of screens with different optical properties describing the blur in powder phosphors using the diffusion-limit conditions for the optical transport. These expressions have been used in the literature to model imaging systems (see for instance Van Metter and Rabbani, 1990; Nishikawa and Yaffe, 1990). Analogous theoretical solutions for transparent phosphors were described in detail by Gasper (Gasper, 1973), Barrett (Barrett and Swindell, 1996) and Lubberts (Lubberts, 1968). Lubberts used analytical models of spread functions corresponding to light bursts from X-ray interactions that were applicable to homogeneous “idealized” screens consisting of a transparent crystal layer. In this case, the depth-dependent point-spread function P (r, z) of light diffusion modelled (Lubberts, 1968) as:

$$P(r,z)=\frac{z}{4\pi(z^2+r^2)^{3/2}} \quad (3)$$

where, z represents the depth of interaction, and r is the radial dimension describing the distance away from the interaction site. The analytical description of *MTF* and normalized noise power spectrum (*NNPS*) is also possible for turbid granular phosphors with more complex scattering characteristics, using analytical approximations to the general light diffusion equations proposed by Swank (Swank, 1973). For instance, a general model for the depth-dependent MTF for a turbid phosphor in a front-screen configuration is given by (Van Metter and Rabbani, 1990):

$$\mathrm{MTF}(v,z)=\frac{\kappa\rho_1[(b+\kappa\rho_0)e^{bz}+(b+\kappa\rho_0)e^{-bz}]}{(b+\kappa\rho_0)(b+\kappa\rho_1)e^{b\tau}-(b-\kappa\rho_0)(b-\kappa\rho_1)e^{-b\tau}} \quad (4)$$

where, κ represents the reciprocal of the relaxation length describing the scattering and absorption occurring in the phosphor, $b = (\sigma^2 + 4\pi^2\nu^2)$ with σ being the reciprocal of the mean absorption length, $\rho_i = (1 - r_i)/(1 + r_i)$ is the reflectivity of the back and sensor surfaces of the screen at the X-ray entrance ($i = 0$) or at the output ($i = 1$) interfaces, and τ is the thickness. In addition to describing the depth-dependent *MTF*, Eq. 4 can be used to calculate the overall signal and noise transfer functions [34] by integrating Eq. 2 over thickness with the appropriate weighting factors corresponding to the X-ray interaction and light collection at each depth (Van Metter and Rabbani, 1990). This approach has shown good agreement between model predictions and experimental measurements of MTF(Nishikawa and Yaffe, 1990). An investigation into this effect for columnar scintillator screens (Jing *et al.*, 1992; Nagarkar *et al.*, 1998) used in current indirect breast imaging detectors with MC techniques can be found in (Badano *et al.*, 2004).

An alternative approach to obtain analytical approximations has been described by Freed *et al.* (Freed *et al.*, 2010). The approach consists of a physics-based, analytical model to compute detector response functions incorporating a description of the depth effects. The model describes the dependence of the response with X-ray energy, thickness of the transducer layer, and incidence angle of the X-ray beam. Using this framework, detector response functions can be generated in a fraction of a second on any modern, single-CPU computer. The results for indirect detectors have been shown to match MC predictions, which require several hours of computing on a 780-node cluster. The approach relies on *a priori* knowledge of the transport of secondaries using several simplifications needed for the model to be solvable. Firstly, X-ray attenuation in the active material is described as linear with respect to depth of interaction. This is an approximation to the exponential behavior of X-rays which becomes less problematic at higher X-ray energies. Secondly, the signal spread at each depth of interaction is represented by a Lorentzian function with a width at each depth described by a linear fit to data obtained from MC simulations. Finally, the collection efficiency (the fraction of secondaries, in this case, optical photons, that contribute to the detector signal) is approximated with a linear model. For more detail regarding the assumptions, the readers are referred to (Freed *et al.*, 2010). Finally, a relaxation of the values of the coefficients within a fitting procedure to match detector responses obtained from MC is described. This procedure relies on the availability of MC data and allows the model to adjust the spread of the response when additional blur from secondary photons (Compton and fluorescent events) becomes significant. In addition, this procedure allows for compensation of other factors such as inter-columnar crosstalk in CsI:Tl screens. A variant of this model was used to theoretically compare the performance of direct and indirect X-ray imaging detectors (Badano *et al.*, 2011).

A different analytical approach was reported by Evans et al for scintillation detectors in EPIDs or MVCT scanners (Evans *et al.*, 2006). Light output from single, thick scintillators with small cross-sectional area, irradiated with megavoltage X-rays, was modelled

analytically using numerical integration. They modelled a cuboid crystal with a specular exit face and coated with a Lambertian reflector on the other 5 faces as a Lambertian light guide (LLG), mainly based on the fact that scintillators are highly transparent to their own characteristic light. In the LLG model, the light guide is divided into several cells along its length. Light propagation depends on the mean solid angle of each cell and the end faces subtended at the other cells and faces, plus the angular light distribution. The model uses an iterative matrix approach to transport optical photons by considering a vector describing the distribution of optical photons with one element for each cell, plus the entrance face and the optical sensor outside the crystal. Following isotropic light generation within each cell, probabilities of transport from one cell to the next, non-absorption in the faces of each cell, volume attenuation within the crystal of each cell, Lambertian-reflected light reaching the next cell, and scattered light from the faces of each cell reaching the exit face are calculated separately. The model also addresses the special cases of the two end faces. For more detail regarding the mathematical methods used in the model, the readers are referred to Ref. (Evans *et al.*, 2006). The LLG model was benchmarked for speed and accuracy against an existing optical MC code (Mosleh-Shirazi *et al.*, 1998b) by modelling CsI(Tl) crystals of 1.5 × 1.5 and 3 × 3 mm^2 cross-section and up to 10 mm thickness.

3.2 Monte Carlo methods

Numerical approaches that allow for arbitrary geometries are essential tools for the study of light-emissive radiation detectors. Among them, MC techniques are particularly well positioned for tracking independent optical quanta transport processes in complex geometries. Several MC approaches exist for modelling indirect detectors including ionizing radiation transport and subsequent optical transport. Moisan *et al.* (Moisan *et al.*, 1997; Vozza *et al.*, 1997) developed an MC simulator for PET imaging detectors utilizing the Gamma-Ray Interaction Tracking (GRIT) for high energy photons and DETECT (Knoll and Knoll, 1988) for optical transport calculations. More sophisticated gamma- and X-ray simulations can be achieved by replacing GRIT with more advanced programs including GEANT4, EGSnrc, or PENELOPE (Agostinelli and others, 2003; Kawrakow and Rogers, 2000; Salvat *et al.*, 2006). Blakesley *et al.* performed work in the area of modelling organic X-ray imagers utilizing EGSnrc. The DOSxyznrc code was used to generate the photon absorption probability distribution function and the optical photon transport was modelled by DETECTII routines (Fasbender *et al.*, 2003; Kausch *et al.*, 1999; Radcliffe *et al.*, 1993). More recently, Poludniowski and Evans modelled the light transport in powdered-phosphor scintillator screens using a combined method based on the Boltzmann transport equations (Poludniowski *et al.*, 2013a; Poludniowski *et al.*, 2013b). The three-dimensional dose distribution was calculated using DOSRZnrc. This approach has the advantage of faster calculation times compared to ray tracing or MC methods, but has limitations in modelling the absorbed fraction and MTF for higher binder-to-phosphor relative refractive indices and screen thickness.

A series of in-house optical MC codes has been developed for the specific application of EPID and MVCT detector optimization (although the codes can be applicable to other fields too). The model of a scintillator detector element in the shape of a rectangular parallelepiped, originally coded in XL FORTRAN, accepts the pre-computed depth-dose

distribution resulting from the incident ionizing radiation as input (Mosleh-Shirazi *et al.*, 1994, 1998b). It then generates the corresponding number of optical photons isotropically based on the scintillator light yield. The detector element has configurable dimensions, scintillator material, coating type (specular or Lambertian) and reflectivity, combinations of coating types on different crystal faces, and distance to the optical receptor. In addition to providing various quantities during the transport of the scintillation light within the detector element, the outputs include the number and spatial distribution of the optical photons reaching the optical receptor. The code was revised and rewritten later in the MATLAB environment, expanded to add the ability to model a 2D array of coated detector elements each in the shape of a rectangular parallelepiped with optical crosstalk, and called ScintSim1 (Mosleh-Shirazi *et al.*, 2014a). The updated code (ScintSim2) includes the ability to model divergent 2D arrays of coated detector elements (Mosleh-Shirazi *et al.*, 2014b). The same group also used GEANT4 to model a parallel-element 2D array of coated scintillators that includes X-ray, electron and optical photon transport (Ranjbar, 2015).

Researchers in various fields continue to develop in-house MC codes highly tailored to their investigations. For instance, in PET imaging simulations, Roncali *et al.* reported on the use of surface roughness measurements to affect the angular distribution of reflections within a bulk crystal (Roncali and Cherry, 2013b; Roncali *et al.*, 2014). Another Moxysulfide screens bonded to a metal plate X-ray converter in a video-based EPID. Their model assumed the screen to be a weakly absorbing medium and included some optical processes (Radcliffe *et al.*, 1993).

Few MC codes are available freely as open source packages. Among them, the GEANT4 and GATE (Agostinelli and others, 2003; Jan *et al.*, 2004) toolkits for particle transport are widely used. Although the main applications are in high energy, nuclear and accelerator applications, some investigators have used GEANT4 for the modelling of light transport in radiation detectors (Meo *et al.*, 2009; Bobin *et al.*, 2010; van der Laan *et al.*, 2010a; Hirano *et al.*, 2012; Ranjbar, 2015; Ghadiri and Khorsandi, 2015; Játékos *et al.*, 2016; Bobin *et al.*, 2016). GATE (Geant4 Application for Tomographic Emission) focuses more on nuclear imaging and radiotherapy with a scripted user interface. Until now, optical transport in GEANT4 and GATE was based on DETECT 2000 (Levin and Moisan, 1996). Several models are available that describe both the crystal surface and the material (e.g. reflector) in contact with that surface. The POLISH model assumes a perfectly flat, polished surface that reflects photons in a specular manner, based on Fresnel equations. In contrast, the GROUND model can be used to represent a rough surface, in which the surface is considered as microfacets, the orientations of which with respect to the surface normal follow a Lambertian distribution. Both models are unrealistic representations of the surface; to provide more flexibility to users, an alternative called the UNIFIED model was developed and is available in GEANT4. This model assumes that the microfacet angles follow a Gaussian distribution which can be parameterized by the user, and that the type of reflections can be chosen using four probabilities. Though the UNIFIED model is more refined than the two other options, it becomes complex to use because of the numerous required input parameters that are often difficult to estimate by the user. This typically results in inaccurate computation of the light transport (Bea *et al.*, 1994b; Janecek and Moses, 2010; Roncali and Cherry, 2013a). More accurate models were developed and have

being implemented in GEANT4 (Janecek and Moses) and GATE (Roncali and Cherry, 2014; Roncali *et al.*, 2017). Janecek and Moses have developed a custom apparatus with an array of photodiodes to measure the 3D reflectance of a crystal illuminated with a laser which angle of incidence is varied from 0 to 90°. They have measured BGO crystals with three different surface finish and shown that (i) a mechanically polished behaved almost perfectly like an ideal flat surface (solid gray line), and (ii) that etching and rough cut finishes dramatically change the reflectance as a function of incidence angle, increasing the reflection at low angles and smoothing the transition to total internal reflection. Roncali and Cherry (Janecek and Moses, 2009; Roncali and Cherry, 2013a) also obtained similar results using a computational approach. Equally important to the probability of reflection is the distribution of reflected light. The direction of the reflected light can change the number of reflections that photons undergo on their way to the photodetector face by either helping in redirecting them toward the photodetector, or sending them backwards (resulting in an increased number of reflections per photon). This will change the total number of detected photons (light output), energy resolution, and transit time in the crystal.

Raytracing software such as Zemax have been used to study light propagation and collection in scintillation detectors (Bauer *et al.*, 2009), but their description is beyond the scope of this review, which mainly focuses on MC methods.

Furthermore, extensive work has been published by Badano *et al.* on modelling indirect X-ray detectors by interfacing PENELOPE with DETECTII routines (Badano and Sempau, 2006; Freed *et al.*, 2009). This open-source model called MANTIS accounts not only for X-ray photon interactions but also for secondary electron interactions and the associated spreading that further degrades detector performance. The optical model takes into account the gain variance due to conversion as a Poisson random variable. The model also supports a realistic columnar model of CsI structures.

One of the major limitations of modelling X-ray imaging scintillators is the geometrical complexity of the film structures. When these structures are not present or significantly simplified, transport of optical quanta becomes computationally more efficient. CartesianDETECT2 (Sharma *et al.*, 2012) is an example of a dedicated MC optical transport tool available especially for pixelated Cartesian geometry detector structures used in PET and SPECT imaging. It is based on the DETECT2 routines but utilizes less memory to model large area detectors as compared to DETECT2. Columns arranged in a grid are identified by their position indices and thus do not require to be stored in memory. To facilitate the set up and execution of computational experiments with columnar scintillator simulations, Dong *et al.* reported a graphical user interface for hybridMANTIS, called visualMANTIS that allows for real-time visualizations of the simulation results. visualMANTIS is built using OpenGL and Fast Light Toolkit which provides interactive visualization. Figure 6 shows the screen captures of the tool. A comparison of available packages and literature reports on modelling scintillator-based imaging detectors is presented in Table 2.

3.3 Approaches for validation

3.3.1. X-ray imaging—The predictions of MC light transport codes can be validated against experimental measurements. One approach for X-ray imaging is to compare measured and simulated point-response functions [46]. However, focusing on reproducing summary measures of detector performance (*i.e.*, MTF) might not provide sufficient evidence for model validation (Zhao *et al.*, 2004). Since most models include parameters that can be adjusted to match experimental results, a more sound approach for validating indirect X-ray imager models should compare blur estimates while maintaining the information or Swank factor and light output consistent with previously published data as described in (Freed *et al.*, 2009).

3.3.2. Nuclear imaging and scintillation detectors—One of the main challenges to validate models of light transport in scintillators is the limited information that can be measured experimentally (Bea *et al.*, 1994a; Janecek and Moses, 2010; Bauer *et al.*, 2009; Roncali and Cherry, 2013a). Primary validation measurements include light output of single crystals of different sizes, orientation, surface treatment, and reflector type. Inaccuracies will also be apparent when studying timing properties of scintillator as often done for PET detector design (see section 4.2).

3.3.3. Radiotherapy imaging systems—Radiotherapy imaging for treatment verification is no exception, and validation is also challenging in optical MC for this application. Mosleh-Shirazi compared outputs from individual modules of their code (e.g., polar angle probability densities for a Lambertian reflector, Fresnel coefficients of reflection, etc.) with expected theoretical results (Mosleh-Shirazi, 1997). Experimental validation of the relative light outputs of individual scintillator cubes with different materials (CsI(Tl), BGO and $ZnWO_4$) and coatings (specular and Lambertian) was also presented. For the subsequent developments of the code (Mosleh-Shirazi *et al.*, 2014a; Ranjbar, 2015), individual optical modules were checked against theory and the results of the first version.

3.4 Computational efficiency

A typical X-ray imaging problem can consist of a flux of 10^{10} X-rays per mm^2, forcing the code to record and analyze in the order of 10^{25} events including the transport of all secondary particles and the interaction of the particles with the medium. The disadvantage of long simulation time has been addressed with the development of hybridMANTIS for parallelizing simulations using GPUs (Sharma *et al.*, 2012) (Figure 7). hybridMANTIS is a modified version of MANTIS with improved geometrical description. The current version of hybridMANTIS uses PENELOPE for X-ray and electron transport and fastDETECT2 for the optical photon transport. hybridMANTIS uses a multiple platform implementation to run X-ray/electron transport in parallel with the optical transport using CPU and GPU processors to achieve significant improvements in computational efficiency. In this work, the penEasy (Sempau *et al.*, 2011) main program was modified to output energy deposition locations and energy deposited per event, which is then used by fastDETECT2 to sample the number of optical photons from a Poisson distribution. fastDETECT2 can be used with any x- ray/electron transport package. Apart from improved computational performance, hybridMANTIS also has two significant new features (on-the-fly geometry and columnar

crosstalk) to improve on the realism of columnar array structures in detectors. hybridMANTIS achieves a speed-up factor of up to 627 when compared to MANTIS running in CPUs. Effectively, this approach can analyze in the GPU all optical photon histories generated by the CPU within the same time it takes the CPU to perform the X-ray and electron transport.

4 Applications of optical transport modelling to medical imaging

Optical transport is useful in the research and development of new radiation imaging system configurations. In this section, we describe some of the most important applications of the use of optical transport modelling in the areas of radiological, nuclear, and therapy imaging systems.

4.1 Radiology

MC methods have been instrumental in the understanding of the effect of detector performance in three-dimensional breast imaging applications in particular. Three-dimensional imaging of the breast improves detectability of breast cancer lesions by removing overlaying normal anatomical structures that complicate the visual task in mammography (Boone et al., 2005; Gong et al., 2006; Knoll and Knoll, 1988; Kwan et al., 2007; Yang et al., 2007). However, the design and optimization of 3D breast imaging systems requires an in-depth understanding through theory, simulation, and experimentation of the underlying physical processes that determine image quality. The effect of oblique X-ray incidence in breast tomosynthesis systems was described using MC tools (Badano et al., 2011) consistent with experimental measurements reported by Mainprize et al. (Mainprize et al., 2006), which show significant decreases in MTFs under oblique X-ray incidence angle for an indirect full-field digital detector. Within this framework, knowledge of the response of the detector can be precalculated with MC methods and incorporated into iterative image reconstruction methods.

4.2 Nuclear imaging

Similarly to radiology, light transport and light collection is a critical aspect of nuclear imaging detector design. While scanner performance depends on several factors, it is primarily controlled by the detector that converts high energy radiation into visible light that is collected by a photodetector. Light transport in the scintillator thus plays a key role in defining detector performance and ultimately determines the spatial resolution, energy resolution, timing resolution and depth-of-interaction (DOI) resolution of nuclear medicine detectors. Light transport is dependent on the crystal geometry, the bulk absorption and scattering properties of the material, the surface treatment of the crystal faces, the reflector possibly attached to the scintillator, and other materials used to couple components (glues).

Some aspects of scanner performance (e.g., sensitivity, count rate) can be studied with MC simulation without a detailed model of the detector physics. However, certain characteristics including timing and spatial resolution cannot be properly assessed without an accurate model of the components including the light transport. For example, time-of-flight (TOF) PET scanners require subnanosecond resolution (Moses, 2003) which can only be achieved

with detailed understanding of the light transport contribution to detector timing. Light transport is also important for DOI-encoding detectors using unpolished crystals with a rough surface (Moses and Derenzo, 1994; Yang *et al.*, 2006) which are increasingly used in preclinical and clinical scanners. Rough surfaces have complex interactions with incident light due to large variations in surface height and orientation. Optimization of DOI or TOF detectors cannot be carried out using simplistic reflectance properties and requires accurate crystal reflectance models such as those developed by Janecek and Moses, or Roncali *et al.* (Stockhoff *et al.* 2017).

4.3 Radiotherapy imaging

Verification that the patient's anatomy remains as planned with respect to the beams is normally done on the accelerator by electronic portal imaging or CT. Cone-beam kVCT is often performed by employing an additional X-ray tube and an imager positioned orthogonally to the treatment axis (Evans, 2008). Despite the wider use of image-guided radiotherapy devices using kilovoltage x-rays, to the best of our knowledge, no papers on optical MC on such systems have been published. Optical modelling work has been carried out on thick scintillators for megavoltage imaging. The low detection QE at high photon energies necessitates a thick scintillator, for which segmented crystals were proposed to preserve spatial resolution (Mosleh-Shirazi *et al.*, 1994) (Figure 1).

A study to optimize the design of segmented scintillator arrays using an in-house optical MC code and experimental measurements investigated the effects of scintillator type, detector element size, crystal coating type and reflectivity, combinations of different coatings on detector faces, scintillator doping level, and crystal transparency on light output magnitude and/or angular distribution (Mosleh-Shirazi *et al.*, 1998b). A substantial improvement in the optical coupling efficiency of video-based EPIDs was predicted by an analytical LLG model and the above-mentioned optical MC code with the mirror-lens-camera combination replaced by an amorphous silicon flat panel (Evans *et al.*, 2006). Recently, the ScintSim1 code was benchmarked against the corresponding GEANT4 model of a segmented scintillator array (Ranjbar, 2015). Also, the ScintSim2 code was used to demonstrate that when optical transport is included, the LSF and MTF performance of parallel-or divergent-element, segmented arrays are sufficiently different from their corresponding non-optical simulation results, to conclude that the additional effort put into optical modelling is worthwhile (Mosleh-Shirazi *et al.*, 2014b).

Another group has reported using the DETECT2000 MC code and measurements to study detector design parameters for MVCT employing segmented scintillator arrays coupled to photodiodes (Monajemi *et al.*, 2004). The same group later used both X-ray and optical MC simulations to study the effects of crystal height, septa material, beam divergence, and beam spectrum on MTF and zero frequency DQE of 2D arrays of $CdWO_4$ crystals and photodiodes. When the effect of optical photon transport was considered, the presence of divergence caused loss of spatial resolution and appeared to spatially shift the input signal (Monajemi *et al.*, 2006).

Others have incorporated optical MC in their studies of segmented arrays for use in EPIDs using the DETECT2 code. Wang *et al.* examined the effects of considering optical transport

when replacing a conventional phosphor screen by a 2D scintillator array, coupled to an amorphous silicon flat panel. They concluded that optical Swank factor and DQE were normally weakly affected by absorption and scattering but with very thick detectors or small element pitch, they were significantly degraded by optical effects (Wang *et al.*, 2009). Data derived from published outputs of optical MC models have also been used, for example, to calculate the average optical photon yield (Radcliffe *et al.*, 1993) for the modelling and optimization of an EPID (Bissonnette *et al.*, 1997a; Bissonnette *et al.*, 1997b).

5 Next generation simulators

From basic concepts to the description of available software tools and applications, it is clear that light transport modelling presents numerous challenges for generic or specific applications. Future developments in optical MC models may take place in at least three ways: (i) improvements specific to each application, (ii) better integration in models with less parametrization by the user, and (iii) more unified, multi-purpose, generic codes that can be used in different fields.

5.1 Improvements for specific applications

Because of the different applications within each imaging modality, different models of light transport and technical complexity are involved. Nuclear medicine is one of the major research areas in which light transport in scintillation detectors needs to be accurately modelled. In the last 10 years, PET technology has been completely transformed by the integration of time-of-flight (TOF) information that has greatly enhanced image contrast, and has strongly pushed for improved timing resolution. These developments require fine optimization of the detectors, and create the need for more accurate optical models. Recent studies demonstrated detector timing resolution as low as 100 ps (Schaart *et al.*, 2010; Gundacker *et al.*, 2013), and indicate that an absolute understanding of all timing components will be needed to progress further. The recent experimental work of Weele *et al.* (Weele *et al.*, 2015a, b) describes an in-depth study of light transit time and indicates several promising research directions. The second paper from ter Weele et al. published at the same time illustrates the limitations of simulations when studying crystals that are not perfectly polished. With respect to timing resolution, there has been great progress on utilizing detection of the Cerenkov light produced by recoil electrons in the scintillator (Lecoq *et al.*, 2010). Due to the extremely low yield of Cerenkov photons, detection of these photons requires an optimal light collection (i) in the scintillator and (ii) at the interface scintillator-photodetector (Somlai-Schweiger and Ziegler, 2015).

The photodetector is often not modelled or just represented by its quantum efficiency. However, this component should be incorporated into light transport models because of the multiple reflections at the interface crystal-photodetector. It also plays a large role in determining the timing resolution. Some groups have developed sophisticated models of the photodetector pulse response (Seifert *et al.*, 2012; Tabacchini *et al.*, 2014), but not integrated in simulation packages and only considering the photodetector triggering and charge conversion processes without taken into account optical coupling. This creates an additional source of uncertainty in optical simulations. Lastly, there is a growing interest in using

nuclear imaging (PET and collection of Cerenkov light) for radiotherapy for dose verification in particular (Glaser *et al.*, 2014). Recent research integrating PET into the proton therapy machine (in beam PET) requires a scanner and detector architecture different than that of traditional PET systems for geometry and performance constraints (Sportelli *et al.*, 2014; Shao *et al.*, 2014).

In the field of radiotherapy imaging, realistic models of the various optical sensors used to collect scintillation light can be useful toward increasing accuracy and applicability of optical MC models that can be used more widely as quantitative tools (e.g., EPID dosimetry and scintillator arrays coupled to active-matrix flat-panel imagers). MC-based EPID dosimetry research and clinical applications will also be greatly aided by easier import of complex media geometries and materials including patient anatomical details from CT scans. Other desirable developments include allowing more complex detector geometries, simulating detectors suitable for cone-beam kVCT at the time of treatment, and better tools to visualize the output of optical MC codes.

5.2 Integrated models

One of the major limitations in existing codes based on DETECT and in-house tools is the complexity of the model and how to properly parameterize it. For example, the UNIFIED model available in GATE requires the user to select one parameter to describe the orientation of the microfacets (the so-called sigma-alpha) and four probabilities of reflections. While the orientation of the microfacets can be obtained from 2D profilometer measurements, it is nearly impossible for a user to properly set these probabilities that cannot be measured directly or indirectly. New approaches intend to limit the number of input parameters left to the user, potentially limiting the risk of errors and making the model easier to use.

When the user input requirements of optical MC models are compared to those of ionizing radiation codes such as MCNP, EGS, etc., a major difference exists in the extent to which the user is required to parameterize the material properties. Optical MC models are not mature enough yet to be able to accept materials in the same manner as their ionizing radiation counterparts and then compute or have access to the interaction cross-sections, probabilities and other parameters themselves. For example, to simulate the transport of x- or gamma-rays using well-established ionizing radiation MC codes, the user usually defines each material by its chemical composition and density. The code then calculates interaction cross-sections and other relevant radiation quantities from its libraries based on the energy spectra of the photons or electrons being transported. In contrast, in current optical MC codes, users have to input several parameters like volume attenuation and surface reflection coefficients, refractive index, etc. Although this provides opportunity to control and set such parameters, the model's results can become highly dependent on the values of the parameters used which leads to uncertainty in the output. A desirable scenario is that the user selects a scintillation material (e.g., NaI(Tl)), and its geometry, and the code proceeds with the simulation by looking up the required optical transport properties.

Another aspect of simulators that would be useful for investigations of optical transport in imaging is the ability to report estimates of uncertainties associated with the quantities of interest. Uncertainty in MC transport can be categorized as systematic and statistical.

Systematic errors are due to approximate models or to uncertainty in the definition of the material and surface properties. On the other hand, statistical uncertainty is associated with a finite number of histories. Understanding of the uncertainties in the quantities of interest is crucial for determining the effect of different design parameters and to guide the more focused experimental confirmation of the simulation predictions. Even though it is common to observe experimental uncertainties larger than those of simulation results, the reporting of uncertainty estimates is an aspect of simulation packages that will benefit the community.

Monte Carlo optical transport simulations would also benefit from utilizing variance reductions techniques that are common in transport methods for other types of particles and problems. Although some effort has been placed on understanding the variance components of optical transport simulation (see for instance Gutierrez *et al.*, 2014), more research is needed to facilitate the use of variance reduction techniques to speed up optical transport while ensuring unbiased estimates of the quantities of interest for the different simulation experiment.

Finally, the complexity of the models is often aggravated by the lack of documentation which makes the understanding and usability of the code and choice of input parameters even more challenging while decreasing the reproducibility of modelling results.

5.3. Toward a unified simulation package?

Specialization is what makes the development of unified, generic tools difficult. A number of development and improvements may, however, lead to unified, multi-purpose optical MC codes that can be used across applications. Integrating a major part of optical codes in popular simulation packages such as GEANT4, GATE, seems to be the most promising approach. Integration of developments for users is now facilitated by the widespread use of collaborative software development tools such as Github. For example, GATE now relies on a platform where contributors can share their developments, that can later be incorporated in future releases (GATE github, 2016). However, there is still a need for generalizable approaches, appropriate documentation, and consistency in output formatting. In addition, a general method of defining geometry and outputs is one of the most important requirements. If codes rely on input and output files that follow the same universal format, interfacing between the optical transport codes and performing intercomparison studies will become easier and more reliable. Adoption of such a universal format by the developers of the ionizing radiation MC codes can further facilitate the interfacing between ionizing and optical radiation transport codes.

References

Agostinelli S, et al. Geant4: A simulation toolkit. Nucl Instrum Meth. 2003; A506:250–303.

Antonuk LE. Electronic portal imaging devices: A review and historical perspective of contemporary technologies and research. Phys Med Biol. 2002; 47:R31. [PubMed: 11936185]

Aristizabal O, Christopher DA, Foster FS, Turnbull DH. 40-MHz echocardiography scanner for cardiovascular assessment of mouse embryos. Ultrasound in medecine and biology. 1998; 24:1407–17.

Badano A, Freed M, Fang Y. Oblique incidence effects in direct X-ray detectors: a first-order approximation using a physics-based analytical model. Med Phys. 2011; 38:2095–8. [PubMed: 21626942]

Badano A, Gagne RM, Gallas BD, Jennings RJ, Boswell JS, Myers KJ. Lubberts effect in columnar phosphors. Med Phys. 2004; 31:3122–31. [PubMed: 15587665]

Badano A, Sempau J. Mantis: Combined X-ray, electron and optical Monte Carlo simulations of indirect radiation imaging systems. Phys Med Biol. 2006; 51:1545. [PubMed: 16510962]

Baranov V, Filchenkov V, Konin A, Zhuk V. A study of the characteristics of scintillation detectors with a diffuse reflector. Nucl Instrum Methods Phys Res A. 1996374:335–40.

Barrett, HH., Swindell, W. Radiological imaging: The theory of image formation, detection, and processing. San Diego: Academic Press; 1996.

Bauer F, Corbeil J, Schmand M, Henseler D. Measurements and ray-tracing simulations of light spread in LSO crystals. IEEE Trans Nucl Sci. 2009; 56:2566–73.

Bea J, Gadea A, Garcia-Raffi L, Rico J, Rubio B, Tain J. Simulation of light collection in scintillators with rough surfaces. Nucl Instrum Methods Phys Res A. 1994a; 350:184–91.

Bea J, Gadea A, Garcia-Raffi LM, Rico J, Rubio B, Tain JL. Simulation of light collection in scintillators with rough surfaces. Nucl Instrum Methods Phys Res A. 1994b; 350:184–91.

Berg E, Roncali E, Cherry SR. Optimizing light transport in scintillation crystals for time-of-flight PET: An experimental and optical Monte Carlo simulation study. Biomed Opt Express. 2015; 6:2220–30. [PubMed: 26114040]

Berg WF. The photographic emulsion layer as a three-dimensional recording medium. Appl Opt. 1969; 8:2407–16. [PubMed: 20076052]

Bissonnette J-P, Cunningham I, Jaffray DA, Fenster A, Munro P. A quantum accounting and detective quantum efficiency analysis for video-based portal imaging. Med Phys. 1997a; 24:815–26. [PubMed: 9198014]

Bissonnette J-P, Cunningham I, Munro P. Optimal phosphor thickness for portal imaging. Med Phys. 1997b; 24:803–14. [PubMed: 9198013]

Blake SJ, Vial P, Holloway L, Greer PB, McNamara AL, Kuncic Z. Characterization of optical transport effects on epid dosimetry using geant4. Med Phys. 2013; 40:041708. [PubMed: 23556878]

Bobin C, Thiam C, Bouchard J. Calculation of extrapolation curves in the 4π (ls) β-γ coincidence technique with the Monte Carlo code geant4. Applied Radiation and Isotopes. 2016; 109:319–24. [PubMed: 26699674]

Bobin C, Thiam C, Bouchard J, Jaubert F. Application of a stochastic tdcr model based on Geant4 for cherenkov primary measurements. Applied Radiation and Isotopes. 2010; 68:2366–71. [PubMed: 20542706]

Boone JM, Kwan ALC, Seibert JA, Shah N, Lindfors KK, Nelson TR. Technique factors and their relationship to radiation dose in pendant geometry breast CT. Med Phys. 2005; 32:3767–76. [PubMed: 16475776]

Boyer AL, Antonuk L, Fenster A, Van Herk M, Meertens H, Munro P, Reinstein LE, Wong J. A review of electronic portal imaging devices (EPIDs). Med Phys. 1992; 19:1–16. [PubMed: 1620036]

Carel, WEvE. Inorganic scintillators in medical imaging. Phys Med Biol. 2002; 47:R85. [PubMed: 12030568]

Carrier C, Lecomte R. Effect of geometrical modifications and crystal defects on light collection in ideal rectangular parallelepipedic bgo scintillators. Nucl Instrum Methods Phys Res A. 1990; 294:355–64.

Catana C, Wu Y, Judenhofer MS, Qi J, Pichler BJ, Cherry SR. Simultaneous acquisition of multislice PET and MR images: Initial results with a MR-compatible PET scanner. J Nucl Med. 2006; 47:1968–76. [PubMed: 17138739]

Cavouras D, Kandarakis I, Maris T, Panayiotakis GS, Nomicos CD. Assessment of the gain transfer function of phosphors for application in medical imaging radiation detectors. Eur J Radiol. 2000; 35:70–7. [PubMed: 10930770]

Cherry SR, Shao Y, Tornai MP, Siegel S, Ricci AR, Phelps ME. Collection of scintillation light from small BGO crystals. IEEE Trans Nucl Sci. 1995; 42:1058–63.

Cherry, SR., Sorenson, JA., Phelps, ME. Physics in nuclear medicine (fourth edition). (Philadelphia: W.B. Saunders); 2012a.

Cherry, SR., Sorenson, JA., Phelps, ME. Physics in nuclear medicine. Philadelphia: W.B. Saunders; 2012b.

De Belder M, Kerf JD, Jespers J, Verbrugghe R. Light diffusion in photographic layers: Its influence on sensitivity and modulation transfer. JOURNAL OF THE OPTICAL SOCIETY OF AMERICA. 1965; 55:1261–8.

DePalma JJ, Gasper J. Determining the optical properties of photographic emulsions by the Monte Carlo method. Photographic Science and Engineering. 1972; 16:181–91.

Derenzo SE, Choong W-S, Moses WW. Fundamental limits of scintillation detector timing precision. Phys Med Biol. 2014; 59:3261. [PubMed: 24874216]

Derenzo SE, Choong W-S, Moses WW. Monte Carlo calculations of PET coincidence timing: Single and double-ended readout. Phys Med Biol. 2015; 60:7309. [PubMed: 26350162]

Derenzo SE, Riles JK. Monte Carlo calculations of the optical coupling between bismuth germanate crystals and photomultiplier tubes. IEEE Trans Nucl Sci. 1982; 29:191–5.

Derenzo SE, Weber MJ, Bourret-Courchesne E, Klintenberg MK. The quest for the ideal inorganic scintillator. Nucl Instrum Methods Phys Res A. 2003; 505:111–7.

Després P, Funk T, Shah KS, Hasegawa BH. Monte Carlo simulations of compact gamma cameras based on avalanche photodiodes. Phys Med Biol. 2007; 52:3057. [PubMed: 17505089]

Dong H, Sharma D, Badano A. Web-based, GPU-accelerated, Monte Carlo simulation and visualization of indirect radiation imaging detector performance. Med Phys. 2014; 41:121907. [PubMed: 25471967]

Dorenbos P, Haas JTMd, van Eijk CWE. Non-proportionality in the scintillation response and the energy resolution obtainable with scintillation crystals. IEEE Trans Nucl Sci. 1995; 42:2190–202.

Drangova M, Rowlands JA. Optical factors affecting the detective quantum efficiency of radiographic screens. Med Phys. 1986; 13:150–75. [PubMed: 3702809]

Evans PM. Anatomical imaging for radiotherapy. Phys Med Biol. 2008; 53:R151. [PubMed: 18495981]

Evans PM, Mosleh-Shirazi MA, Harris EJ, Seco J. Monte Carlo and Lambertian light guide models of the light output from scintillation crystals at megavoltage energies. Med Phys. 2006; 33:1797–809. [PubMed: 16872087]

Falk F, Sparrman P. A computer method for the evaluation of the optical properties of scintillation detector assembles. Nuclear Instruments and Methods. 1970; 85:253–8.

Fasbender R, Li H, Winnacker A. Monte carlo modeling of storage phosphor plate readouts. Nucl Instrum Methods Phys Res A. 2003; 512:610–8.

Freed M, Miller S, Tang K, Badano A. Experimental validation of Monte Carlo (mantis) simulated X-ray response of columnar CsI scintillator screens. Med Phys. 2009; 36:4944–56. [PubMed: 19994503]

Freed M, Park S, Badano A. A fast, angle-dependent, analytical model of CsI detector response for optimization of 3D X-ray breast imaging systems. Med Phys. 2010; 37:2593–605. [PubMed: 20632571]

Gasper J. Modulation transfer function and efficiency of transparent luminescing materials. JOURNAL OF THE OPTICAL SOCIETY OF AMERICA. 1973; 63:714.

GATE github. 2016. Https://github.Com/opengate/GATE

Ghadiri R, Khorsandi J. Studying the response of a plastic scintillator to gamma rays using the Geant4 Monte Carlo code. Applied Radiation and Isotopes. 2015; 99:63–8. [PubMed: 25725326]

Glaser AK, Zhang R, Gladstone DJ, Pogue BW. Optical dosimetry of radiotherapy beams using Cherenkov radiation: The relationship between light emission and dose. Phys Med Biol. 2014; 59:3789. [PubMed: 24938928]

Gong X, Glick SJ, Liu B, Vedula AA, Thacker S. A computer simulation study comparing lesion detection accuracy with digital mammography, breast tomosynthesis, and cone-beam CT breast imaging. Med Phys. 2006; 33:1041–52. [PubMed: 16696481]

Gundacker S, Auffray E, Frisch B, Jarron P, Knapitsch A, Meyer T, Pizzichemi M, Lecoq P. Time of flight positron emission tomography towards 100 ps resolution with L(Y)SO: An experimental and theoretical analysis. J Instrum. 2013; 8:P07014.

Gutierrez B, Badano A, Samuelson F. Analytic variance estimates of Swank and Fano factors. Med Phys. 2014; 41:072102. [PubMed: 24989397]

Hirano Y, Zeniya T, Iida H. Monte carlo simulation of scintillation photons for the design of a high-resolution spect detector dedicated to human brain. Ann Nucl Med. 2012; 26:214–21. [PubMed: 22160738]

Huber JS, Moses WW, Andreaco MS, Loope M, Melcher CL, Nutt R. Geometry and surface treatment dependence of the light collection from LSO crystals. Nucl Instrum Methods Phys Res A. 1999; 437:374–80.

Hunter WC, Barrett HH, Muzi JP, McDougald W, MacDonald LR, Miyaoka RS, Lewellen TK. Scout: A fast Monte-Carlo modeling tool of scintillation camera output. Phys Med Biol. 2013; 58:3581. [PubMed: 23640136]

Jan, S. IEEE NSS/MIC, GATE User Meeting. San Diego, USA: 2015. Ongoing developments in GATE and what to expect in upcoming versions.

Jan S, et al. GATE: A simulation toolkit for PET and spect. Phys Med Biol. 2004; 49:4543–61. [PubMed: 15552416]

Janecek M, Moses WW. Design of an instrument to measure optical reflectance of scintillating crystal surfaces. IEEE Trans Nucl Sci. 2008a; 55:1381–6.

Janecek M, Moses WW. Optical reflectance measurements for commonly used reflectors. IEEE Trans Nucl Sci. 2008b; 55:2432–7.

Janecek M, Moses WW. Measuring light reflectance of BGO crystal surfaces. IEEE Trans Nucl Sci. 2009; 55:2443–9.

Janecek M, Moses WW. Simulating scintillator light collection using measured optical reflectance. IEEE Trans Nucl Sci. 2010; 57:964–70.

Jatékos B, Gasparini L, Lőrincz E, Erdei G. Validated simulation for LYSO:Ce scintillator based PET detector modules built on fully digital sipm arrays. J Instrum. 2016; 11:P03028.

Jing T, Cho G, Drewery J, Kaplan SN, Mireshghi A, Perez-Mendez V, Wildermuth D. Enhanced columnar structure in CsI layer by substrate patterning. IEEE Trans Nucl Sci. 1992; 39:1195–8.

Kandarakis I, Cavouras D. Modeling the effect of light generation and light attenuation properties on the performance of phosphors used in medical imaging radiation detectors. Nucl Instrum Methods Phys Res A. 2001; 60:412–23.

Kausch C, Schreiber B, Kreuder F, Schmidt R, Dössel O. Monte carlo simulations of the imaging performance of metal plate/phosphor screens used in radiotherapy. Med Phys. 1999; 26:2113–24. [PubMed: 10535628]

Kawrakow I, Rogers D. The egsnrc code system: Monte carlo simulation of electron and photon transport. 2000

Keller BB, Liu LJ, Tinney J, Tobita K. Cardiovascular developmental insights from embryos. Annals of the New York Academy of Sciences. 2007; 1101:377–88. [PubMed: 17303838]

Knoll, G. Radiation detection and measurement. 3rd edition. John Wiley and Sons; New York: 2000a.

Knoll GF, Knoll TF. Light collection in scintillation detector composites for neutron detection. IEEE Trans Nucl Sci. 1988; 35:872–5.

Kolb A, Lorenz E, Judenhofer MS, Renker D, Lankes K, Pichler BJ. Evaluation of geiger-mode APDs for PET block detector designs. Phys Med Biol. 2010; 55:1815–32. [PubMed: 20208095]

Kwan ALC, Boone JM, Yang K, Huang S-Y. Evaluation of the spatial resolution characteristics of a cone-beam breast CT scanner. Med Phys. 2007; 34:275–81. [PubMed: 17278513]

Lecoq P, Auffray E, Brunner S, Hillemanns H, Jarron P, Knapitsch A, Meyer T, Powolny F. Factors influencing time resolution of scintillators and ways to improve them. IEEE Trans Nucl Sci. 2010; 57:2411–6.

Levin A, Moisan C. A more physical approach to model the surface treatment of scintillation counters and its implementation into DETECT. IEEE Nucl Sci Symp Conf Rec. 1996:702–6.

Liaparinos PF, Kandarakis IS, Cavouras DA, Delis HB, Panayiotakis GS. Modeling granular phosphor screens by Monte Carlo methods. Med Phys. 2006; 33:4502–14. [PubMed: 17278802]

Liu L, Antonuk LE, Zhao Q, El-Mohri Y, Jiang H. Countering beam divergence effects with focused segmented scintillators for high dqe megavoltage active matrix imagers. Phys Med Biol. 2012; 57:5343. [PubMed: 22854009]

Lubberts G. Random noise produced by x-ray fluorescent screens. JOURNAL OF THE OPTICAL SOCIETY OF AMERICA. 1968; 58:1475–83.

Mainprize JG, Bloomquist AK, Kempston MP, Yaffe MJ. Resolution at oblique incidence angles of a flat panel imager for breast tomosynthesis. Med Phys. 2006; 33:3159–64. [PubMed: 17022208]

Melcher CL, Schweitzer JS. Cerium-doped lutetium oxyorthosilicate - a fast, efficient new scintillator. IEEE Trans Nucl Sci. 1992; 39:502–5.

Meo SL, Bennati P, Cinti MN, Lanconelli N, Navarria FL, Pani R, Pellegrini R, Perrotta A, Vittorini F. A geant4 simulation code for simulating optical photons in spect scintillation detectors. J Instrum. 2009; 4:P07002.

Miyaoka RS, Xiaoli L, Lockhart C, Lewellen TK. Comparison of detector intrinsic spatial resolution characteristics for sensor on the entrance surface and conventional readout designs. IEEE Trans Nucl Sci. 2010; 57:990–7. [PubMed: 21614135]

Moisan C, Vozza D, Loope M. Simulating the performances of an LSO based position encoding detector for PET. IEEE Trans Nucl Sci. 1997; 44:2450–8.

Monajemi T, Fallone B, Rathee S. Thick, segmented cdwo4-photodiode detector for cone beam megavoltage CT: A Monte Carlo study of system design parameters. Med Phys. 2006; 33:4567–77. [PubMed: 17278808]

Monajemi T, Steciw S, Fallone B, Rathee S. Modeling scintillator-photodiodes as detectors for megavoltage CT. Med Phys. 2004; 31:1225–34. [PubMed: 15191313]

Moses W, Choong W-S, Derenzo S. Modeling time dispersion due to optical path length differences in scintillation detectors. Acta physica Polonica B, Proceedings supplement. 2014; 7:725. [PubMed: 25729464]

Moses WW. Time of flight in PET revisited. IEEE Trans Nucl Sci. 2003; 50:1325–30.

Moses WW, Derenzo SE. Design studies for a PET detector module using a pin photodiode to measure depth of interaction. IEEE Trans Nucl Sci. 1994; 41:1441–5.

Moses WW, Derenzo SE. Prospects for time-of-flight PET using LSO scintillator. IEEE Trans Nucl Sci. 1999; 46:474–8.

Mosleh-Shirazi MA, Evans PM, Swindell W, Symonds-Tayler RJ, Webb S, Partridge M. Rapid portal imaging with a high-efficiency, large field-of-view detector. Med Phys. 1998a; 25:2333–46. [PubMed: 9874825]

Mosleh-Shirazi MA, Swindell W, Evans PM. Monte carlo simulations of CsI (Tl) scintillation crystals for use in a three-dimensional megavoltage CT scanner. Nucl Instrum Methods Phys Res A. 1994; 348:563–6.

Mosleh-Shirazi MA, Swindell W, Evans P. Optimization of the scintillation detector in a combined 3D megavoltage CT scanner and portal imager. Med Phys. 1998b; 25:1880–90. [PubMed: 9800695]

Mosleh-Shirazi, MA. PhD thesis. Institute of Cancer Research University of London; UK: 1997. A combined 3D megavoltage CT scanner and portal imager for treatment verification in radiotherapy.

Mosleh-Shirazi MA, Evans PM, Swindell W, Webb S, Partridge M. A cone-beam megavoltage CT scanner for treatment verification in conformal radiotherapy. Radiotherapy and Oncology. 1998c; 48:319–28. [PubMed: 9925252]

Mosleh-Shirazi MA, Zarrini-Monfared Z, Karbasi S, Zamani A. ScintSim1: A new Monte Carlo simulation code for transport of optical photons in 2D arrays of scintillation detectors. Journal of Medical Physics. 2014a; 39:18. [PubMed: 24600168]

Mosleh-Shirazi MA, Zarrini-Monfared Z, Karbasi S, Zamani A. A new optical photon transport Monte Carlo code for modeling parallel- and focused-element scintillation detector arrays and its use in examination of the full MTF responses of thick segmented scintillators. Physica Medica: European Journal of Medical Physics. 2014b; 30(Suppl 1):e28.

Nagarkar VV, Gupta TK, Miller SR, Klugerman Y, Squillante MR, Entine G. Structured CsI(Tl) scintillators for x-ray imaging applications. IEEE Trans Nucl Sci. 1998; 45:492–6.

Nillius P, Klamra W, Sibczynski P, Sharma D, Danielsson M, Badano A. Light output measurements and computational models of microcolumnar CsI scintillators for x-ray imaging. Med Phys. 2015; 42:600–5.

Nishikawa RM, Yaffe MJ. Effect of various noise sources on the detective quantum efficiency of phosphor screens. Med Phys. 1990; 17:887–93. [PubMed: 2233576]

Ordonez CE, Chang W, Liu J, Gunter DL. Simulation of light output from narrow sodium iodide detectors. IEEE Trans Nucl Sci. 1997; 44:1237–41.

Poludniowski, Gavin G., Evans, PM. Optical photon transport in powdered-phosphor scintillators. Part 1. Multiple-scattering and validity of the boltzmann transport equation. Med Phys. 2013a; 40:041904. [PubMed: 23556898]

Poludniowski, Gavin G., Evans, PM. Optical photon transport in powdered-phosphor scintillators. Part ii. Calculation of single-scattering transport parameters. Med Phys. 2013b; 40:041905. [PubMed: 23556899]

Radcliffe T, Barnea G, Wowk B, Rajapakshe R, Shalev S. Monte carlo optimization of metal/phosphor screens at megavoltage energies. Med Phys. 1993; 20:1161–9. [PubMed: 8413026]

Ranjbar, S. MSc thesis. Shiraz University of Medical Sciences; Iran: 2015. Evaluation of an optical transport model of segmented scintillator arrays for megavoltage x-ray imaging (ScintSim2) using the Geant4 Monte Carlo simulation package.

Rogers D. Fifty years of Monte Carlo simulations for medical physics. Phys Med Biol. 2006; 51:R287–301. [PubMed: 16790908]

Roncali E, Cherry S. Application of silicon photomultipliers to positron emission tomography. Ann Biomed Eng. 2011; 39:1358–77. [PubMed: 21321792]

Roncali E, Cherry SR. Simulation of light transport in scintillators based on 3d characterization of crystal surfaces. Phys Med Biol. 2013; 58:2185–98. [PubMed: 23475145]

Roncali, E., Cherry, SR. IEEE NSS/MIC, GATE workshop. Seattle, WA: 2014. Simulation of light transport in scintillators based on 3d characterization of crystal surfaces.

Roncali E, Schmall JP, Viswanath V, Berg E, Cherry SR. Predicting the timing properties of phosphor-coated scintillators using Monte Carlo light transport simulation. Phys Med Biol. 2014; 59:2023. [PubMed: 24694727]

Roncali E, Stockhoff M, Cherry SR. An integrated model of scintillator-reflector properties for advanced simulations of optical transport. Phys Med Biol. 2017; 62:4811–30. [PubMed: 28398905]

Roncali, E., Kim, CL., McDaniel, DL., Cherry, SR. IEEE Nuclear Science Symposium and Medical Imaging Conference. Seoul, South Korea: 2013. Effect of surface treatment on light transit time in scintillator crystals for PET.

Sabet H, Bhandari HB, Kudrolli H, Nagarkar VV. Proceedings of the 2nd international conference on technology and instrumentation in particle physics (tipp 2011) fabrication of X-ray/gamma-ray detector by growth of microcolumnar CsI:Tl onto silicon photomultipliers. Physics Procedia. 2012; 37:1523–30.

Salvat F, Fernández-Varea V, Sempau J. Penelope-2006: A code system for Monte Carlo simulation of electron and photon transport. OECD Nuclear Energy Agency. 2006

Sawant A, et al. Segmented crystalline scintillators: An initial investigation of high quantum efficiency detectors for megavoltage x-ray imaging. Med Phys. 2005; 32:3067–83. [PubMed: 16279059]

Schaart DR, Seifert S, Vinke R, van Dam HT, Dendooven P, Löhner H, Beekman FJ. Labr3:Ce and SiPMs for time-of-flight PET: Achieving 100 ps coincidence resolving time Phys. Med Biol. 2010; 55:179–89.

Schölermann H, Klein H. Optimizing the energy resolution of scintillation counters at high energies. Nuclear Instruments and Methods. 1980; 169:25–31.

Seifert S, Van Dam HT, Vinke R, Dendooven P, Lohner H, Beekman FJ, Schaart DR. A comprehensive model to predict the timing resolution of SiPM-based scintillation detectors: Theory and experimental validation. IEEE Trans Nucl Sci. 2012; 59:190–204.

Sempau J, Badal A, Brualla L. A penelope-based system for the automated Monte Carlo simulation of clinacs and voxelized geometries-application to far-from-axis fields. Med Phys. 2011; 38(11): 5887–95. [PubMed: 22047353]

Shao Y, Sun X, Lou K, Zhu XR, Mirkovic D, Poenisch F, Grosshans D. In-beam PET imaging for on-line adaptive proton therapy: An initial phantom study. Phys Med Biol. 2014; 59:3373. [PubMed: 24874943]

Sharma D, Badal A, Badano A. Hybridmantis: A CPU-GPU Monte Carlo method for modeling indirect X-ray detectors with columnar scintillators. Phys Med Biol. 2012; 57(8):2357–72. [PubMed: 22469917]

Sharma D, Badano A. Validation of columnar CsI X-ray detector responses obtained with hybridmantis, a CPU-GPU Monte Carlo code for coupled x-ray, electron, and optical transport. Med Phys. 2013; 40:031907. [PubMed: 23464322]

Slates R, Chatziioannou A, Fehlberg B, Taekyeung L, Cherry S. Chemical polishing of LSO crystals to increase light output. IEEE Trans Nucl Sci. 2000; 47:1018–23.

Somlai-Schweiger I, Ziegler SI. Cherencube: Concept definition and implementation challenges of a cherenkov-based detector block for PET. Med Phys. 2015; 42:1825–35. [PubMed: 25832073]

Sportelli G, et al. First full-beam PET acquisitions in proton therapy with a modular dual-head dedicated system. Phys Med Biol. 2014; 59:43. [PubMed: 24321855]

Stockhoff M, Jan S, Dubois A, Cherry S, Roncali E. Advanced optical simulation of scintillation detectors in gate v8.0: First implementation of a reflectance model based on measured data. Phys Med Biol. 2017; 62:L1–L8. [PubMed: 28452339]

Swank RK. Calculation of modulation transfer functions of X-ray fluorescent screens. Appl Opt. 1973; 12:1865–70. [PubMed: 20125622]

Swindell W. The lens coupling efficiency in megavoltage imaging. Med Phys. 1991; 18:1152–3. [PubMed: 1753897]

Swindell W, Evans PM. Scattered radiation in portal images: A Monte Carlo simulation and a simple. physical model Med Phys. 1996; 23:63–73. [PubMed: 8700034]

Swindell W, Morton E, Evans P, Lewis D. The design of megavoltage projection imaging systems: Some theoretical aspects. Med Phys. 1991; 18:855–66. [PubMed: 1961148]

Tabacchini V, Westerwoudt V, Borghi G, Seifert S, Schaart DR. Probabilities of triggering and validation in a digital silicon photomultiplier. J Instrum. 2014; 9:P06016.

van de Hulst, HC. Light scattering by small particles. John Wiley & Sons, Inc; 1957.

van der Laan DJ, Schaart DR, Maas MC, Beekman FJ, Bruyndonckx P, van Eijk CWE. Optical simulation of monolithic scintillator detectors using GATE/Geant4. Phys Med Biol. 2010a; 55:1659. [PubMed: 20182005]

van der Laan DJ, Schaart DR, Maas MC, Beekman FJ, Bruyndonckx P, van Eijk CW. Optical simulation of monolithic scintillator detectors using GATE/geant4. Phys Med Biol. 2010b; 55:1659. [PubMed: 20182005]

Van Eijk CW. Radiation detector developments in medical applications: Inorganic scintillators in positron emission tomography. Radiat Prot Dosimet. 2008; 129:13–21.

Van Metter R, Rabbani M. An application of the multivariate moment-generating functions to the analysis of signal and noise propagation in radiographic screen-film systems. Med Phys. 1990; 17:65–71. [PubMed: 2308548]

Vinke R, Levin CS. A method to achieve spatial linearity and uniform resolution at the edges of monolithic scintillation crystal detectors. Phys Med Biol. 2014; 59:2975. [PubMed: 24841984]

Vozza D, Moisan C, Raquet S. An improved model for the energy resolution of multicrystal encoding detectors for PET. IEEE Trans Nucl Sci. 1997; 44:179–83.

Wang Y, Antonuk LE, El-Mohri Y, Zhao Q. A Monte Carlo investigation of swank noise for thick, segmented, crystalline scintillators for radiotherapy imaging. Med Phys. 2009; 36:3227–38. [PubMed: 19673222]

Wang Y, Antonuk LE, El-Mohri Y, Zhao Q, Sawant A, Du H. Monte Carlo investigations of megavoltage cone-beam CT using thick, segmented scintillating detectors for soft tissue visualization. Med Phys. 2008; 35:145–58. [PubMed: 18293571]

Wang Y, Baldoni G, Rhodes WH, Brecher C, Shah A, Shirwadkar U, Glodo J, Cherepy N, Payne S. Transparent garnet ceramic scintillators for gamma-ray detection. Proc SPIE 8507, Hard X-Ray, Gamma-Ray, and Neutron Detector Physics XIV. 2012:p850717.

Wang Y, El-Mohri Y, Antonuk LE, Zhao Q. Monte Carlo investigations of the effect of beam divergence on thick, segmented crystalline scintillators for radiotherapy imaging. Phys Med Biol. 2010; 55:3659. [PubMed: 20526032]

Weele, DNt, Schaart, DR., Dorenbos, P. Picosecond time resolved studies of photon transport inside scintillators. IEEE Trans Nucl Sci. 2015a; 62:1961–71.

Weele, DNt, Schaart, DR., Dorenbos, P. Scintillation detector timing resolution; a study by ray tracing software. IEEE Trans Nucl Sci. 2015b; 62:1972–80.

Wolfe RN, Marchand EW, Palma JJD. Determination of the modulation transfer function of photographic emulsions from physical measurements. Journal of the Optical Society of America. 1968; 58:1245–56.

Wowk B, Radcliffe T, Leszczynski K, Shalev S, Rajapakshe R. Optimization of metal/phosphor screens for on-line portal imaging. Med Phys. 1994; 21:227–35. [PubMed: 8177155]

Yang K, Kwan ALC, Boone JM. Computer modeling of the spatial resolution properties of a dedicated breast CT system. Med Phys. 2007; 34:2059–69. [PubMed: 17654909]

Yang X, Downie E, Farrell T, Peng H. Study of light transport inside scintillation crystals for PET detectors. Phys Med Biol. 2013; 58:2143. [PubMed: 23470488]

Yang Y, Dokhale PA, Silverman RW, Shah KS, McClish MA, Farrell R, Entine G, Cherry SR. Depth of interaction resolution measurements for a high resolution PET detector using position sensitive avalanche photodiodes. Phys Med Biol. 2006; 51:2131–42. [PubMed: 16625031]

Zhao W, Ristic G, Rowlands JA. X-ray imaging performance of structured cesium iodide scintillators. Med Phys. 2004; 31:2594–605. [PubMed: 15487742]

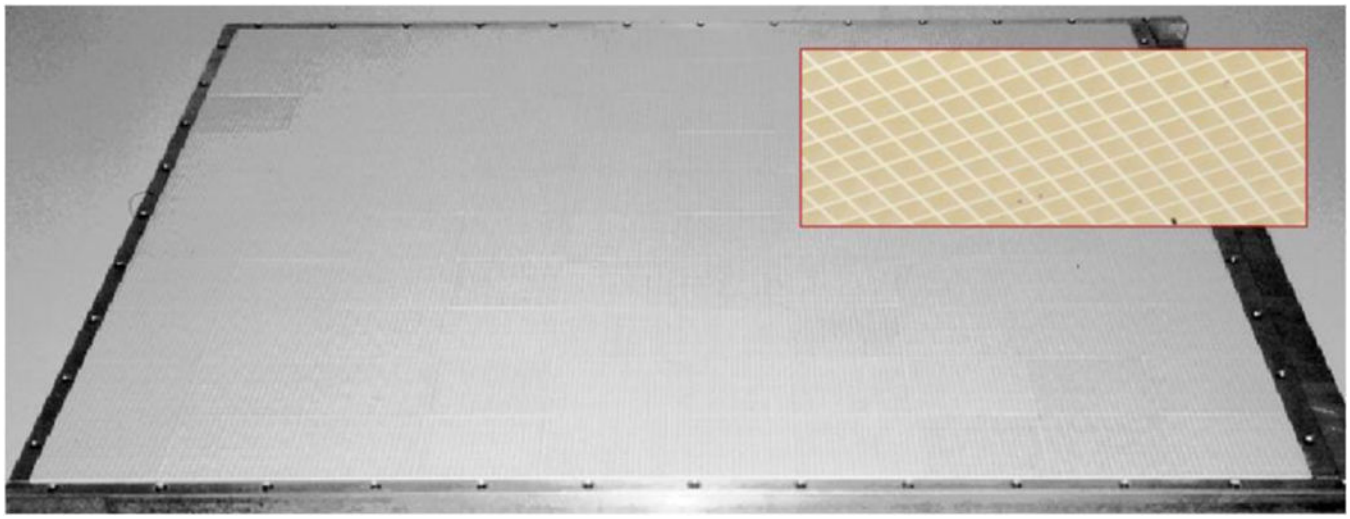

Figure 1.

A 60 × 45 cm^2 area, 1 cm thick, segmented crystalline detector attached to a metal plate for use in megavoltage X-ray imaging. In this example, as shown in the inset, each 3 × 3 × 10 mm^2 detector element is made of CsI(Tl) and is optically isolated. (Mosleh-Shirazi, 1997).

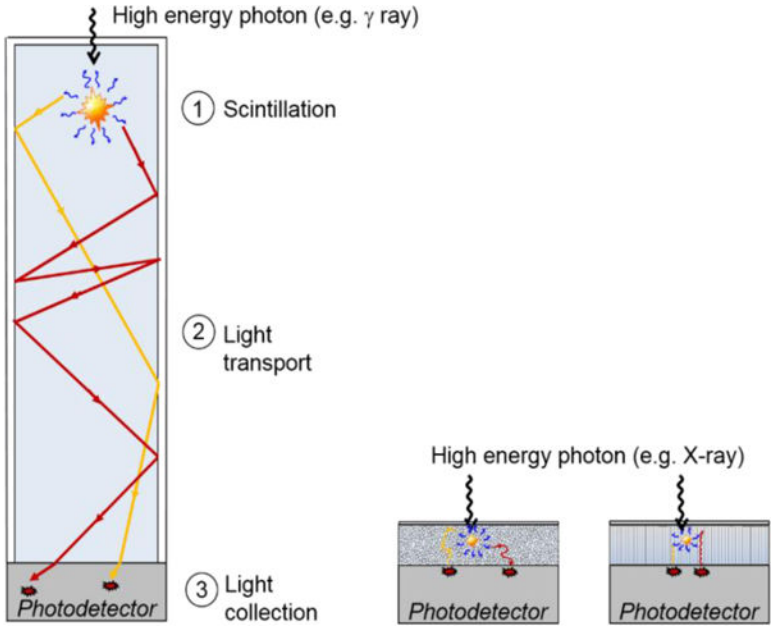

Figure 2.

Scintillation detector. (1) Scintillation: emission of visible light (4,000-50,000 photons/MeV) when incident radiation hits the scintillator. (2) Light transport: the scintillation light travels in the crystal until it reaches the photodetector or escapes. (3) Light collection: the photodetector collects the scintillation light and converts it into an electrical signal, which amplitude is proportional to the amount of detected light. While thick scintillation crystals (10-30 mm) are typically employed in nuclear medicine, phosphor-based detectors (right) are made with a thin layer (~100 μm). Phosphors are granulated (unstructured), or composed of micro columns (structured). Light transport in these phosphors is greatly affected by the internal structure, in contrast to crystalline scintillators.

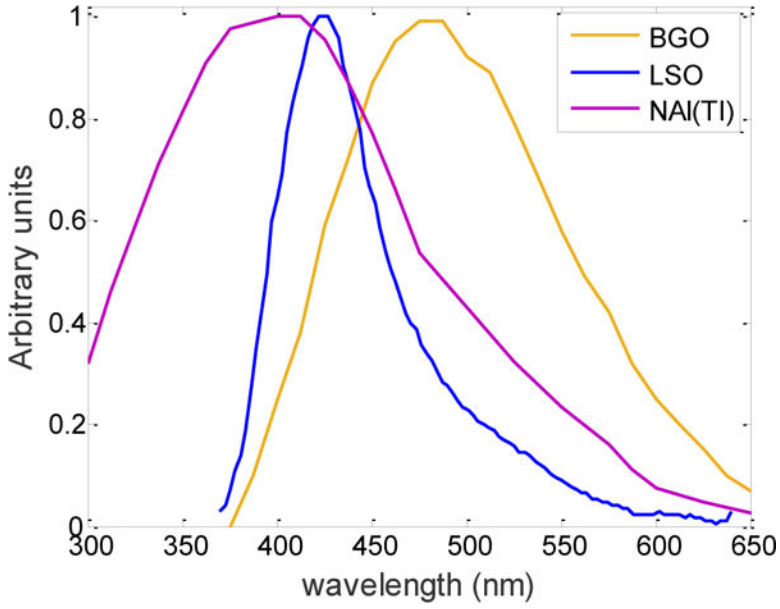

Figure 3.
Emission spectra of three examples of common scintillators: LSO, BGO, and NaI(Tl).

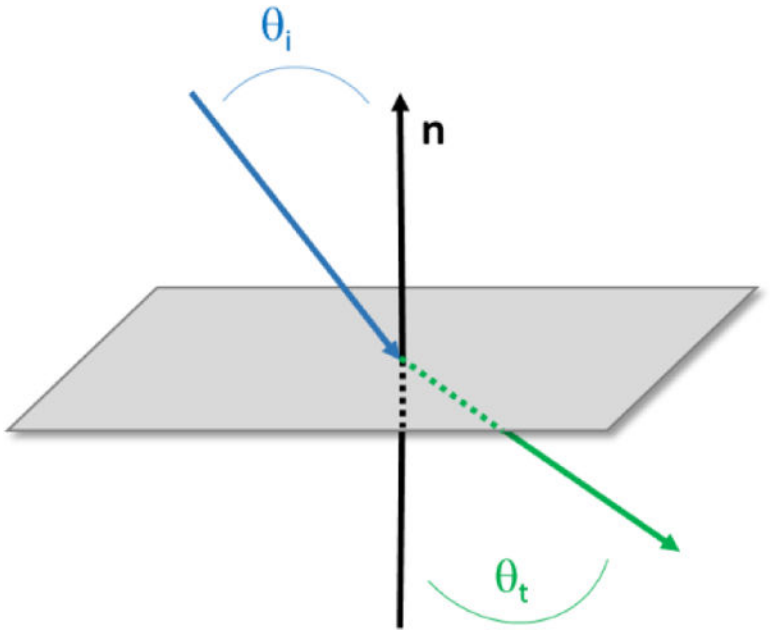

Figure 4.

Reflection on a microfacet on the surface. Incident angle θ_i, local normal n, refracted angle θ_t, reflected angle θ_i.

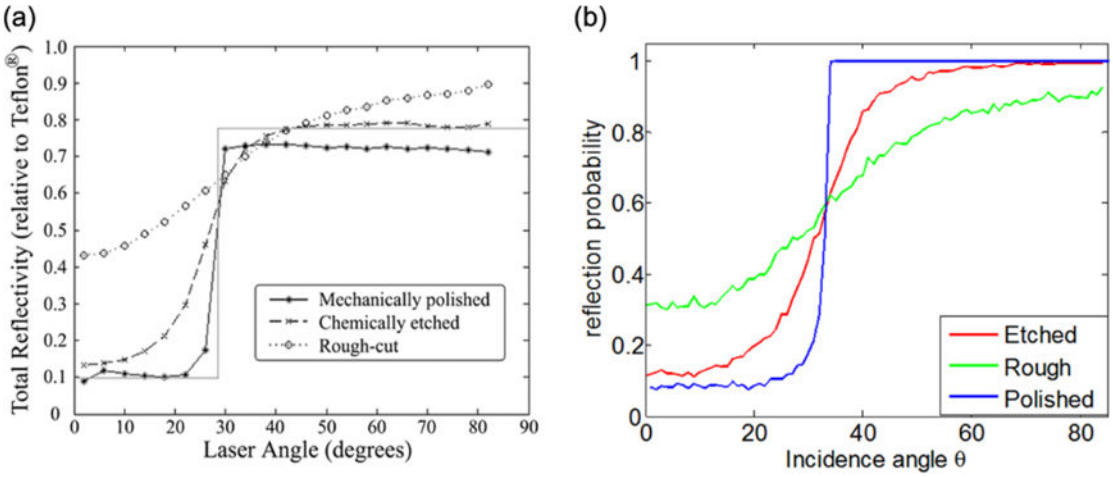

Figure 5.

Reflection properties of rough, etched, and polished crystals. (a) Measurements from Janecek and Moses (Janecek and Moses, 2009). The solid line indicates Fresnel reflection by a perfectly flat surface. (b) Computation from Roncali and Cherry (Roncali and Cherry, 2013a).

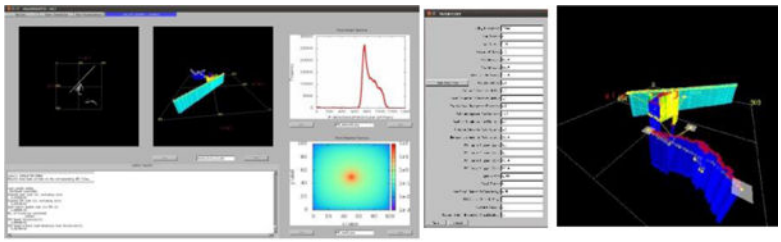

(a) Main screen (b) Input (c) Visualization

Figure 6.

Graphical user interface (GUI) for hybridMANTIS. (a) Main screen showing the pulse height spectrum, optical photon track overlay on top of actual columnar geometry, and point response function (left to right). At the bottom, the code output including the optical transport statistics (like number of photons generated, detected, absorbed, lost etc.) and simulation speed are displayed. (b) Input window to input the optical transport parameters. (c) Visualization window.

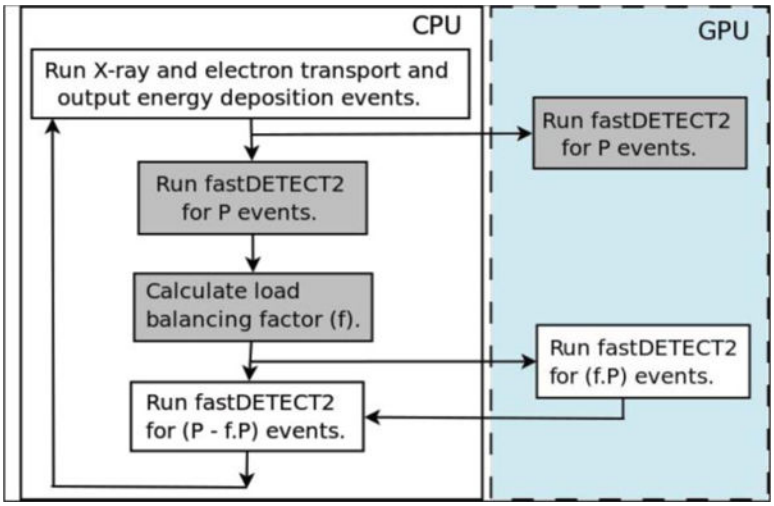

Figure 7.

Mixed-architecture simulation of coupled X-ray, electron, and optical transport in hybridMANTIS using a load balancer. PENELOPE runs in the CPU and outputs scintillation events into a buffer. Once the buffer is full, fastDETECT2 runs in the GPU and in the CPU. A load balancing factor is calculated using relative speeds to optimally distribute load between the GPU and CPU.

Table 1

Main design parameters for imagers that rely on optical transport.

	Gamma Camera/SPECT	PET	X-ray planar imaging	kVCT	MVCT
Detected photons	γ	γ	X-ray	X-ray	X-ray
Energy	100–250 keV	300–600 keV	10–120 kV	10–100 kV	6–25 MV
Material	NaI(Tl), CsI(Tl)	L(Y)SO:Ce, BGO	CsI(Tl), Gd_2O_2S, photostimulable phosphors (columnar)	CsI(Tl), Gd_2O_2S	CsI(Tl), BGO, $CdWO_4$, $ZnWO_4$, NE118
Crystal geometry	• Monolithic, 300–600 mm • 6–12.5 mm thick	• Pixelated: 0.5–4 mm crystals, 20–30 mm thick • Monolithic: 10–30 mm thick	• Unstructured or columnar • Thin “screens”, <1 mm	• Unstructured or columnar • Thin “screens”, <1 mm	Pixelated: 2–3 mm crystals, 10–250 mm thick
Coupling	• Glass window + silicon grease • Optional light guide	• Glued or silicon grease • Optional light guide	Directly deposited or glued, or sandwiched	Directly deposited or glued, or sandwiched	• Remote viewing with air gap • Directly deposited or glued
Photo detector	PMT array	PMT or SiPM array	a-Si photodiode or CCD array, or CMOS backplane	a-Si photodiode or CCD array, or CMOS backplane	• Lens/CCD array • a-Si photodiode array

Table 2

Comparison between freely available open-source research simulation packages for modelling scintillator-based imaging detectors.

	MANTIS	**hybridMANTIS**	**cartesianDETECT2**	**GEANT4**
General features				
Hybrid concept	No	Yes	In preparation	No
GUI	No	Yes	In preparation	Yes
Free download from	https://github.com/DIDSR/	https://github.com/DIDSR	https://github.com/DIDSR/	http://geant4.cern.ch/
X-ray and electron transport				
Code	PENELOPE2006	PENELOPE2006	-	multiple physics packages
Language	Fortran	Fortran	-	C++
Optical transport				
Code	DETECT2	fastDETECT2	cartesianDETECT2	GEANT4 sub-package
Bulk absorption	Yes	Yes	Yes	Yes
Surface reflection	Yes	Yes	Yes	Yes
Surface roughness	Yes	Yes	Yes	Yes
On-the-fly geometry	No	Yes	Yes	No
Columnar crosstalk	No	Yes	No	No
Rayleigh scattering	Yes	No	No	Yes
Wavelength effects	Yes	No	No	Yes
Polarization	Yes	No	No	Yes
Optical sensor	Non-ideal	Non-ideal	Ideal	Ideal
Language	Fortran	C, CUDA[a]	C	C++
Timings				
Code	MANTIS	hybridMANTIS	cartesianDETECT2	GEANT4
Speed (X-ray hist/sec)	1	627	5[e]	

[a] A parallel programming model developed by NVIDIA® Corporation.

[e] Estimated based on equivalent runs for diagnostic energy X-rays (only optical).